ROLE OF INTRAMOLECULAR ELECTROSTATIC INTERACTIONS ON THE KINETICS OF HUMAN CARDIAC MYOSIN β -ISOFORM

by

Akhil Gargey

A dissertation submitted to the faculty of
The University of North Carolina at Charlotte
in partial fulfillment of the requirements
for the degree of Doctor of Philosophy in
Biological Sciences

Charlotte

2021

Approved by:

Dr. Yuri. E Nesmelov

Dr. Andrew Truman

Dr. Valery Grdzelishvili

Dr. Kausik Chakrabarti

Dr. Jerry Troutman

ABSTRACT

AKHIL GARGEY. Role of Intramolecular Electrostatic Interactions on the Kinetics of Human Cardiac Myosin β -Isoform. (Under the direction of DR. YURI. E NESMELOV)

Human cardiac myosin has two isoforms, α and β, sharing significant sequence similarity, but different in kinetics. Small differences in the sequence are responsible for distinct local inter-residue interactions within α and β isoforms, leading to such a dramatic difference in the rate of ADP release. Our analysis of structural kinetics of α and β isoforms using molecular dynamics simulations revealed distinct dynamics in SH1:SH2 helix region, loop 1 region, and loop I289-D324 region of myosin head. We identified permanent salt bridges in these regions on β-isoform, which are not present in the α -isoform. We hypothesized that the isoform-specific electrostatic interactions play a role in the difference of kinetic properties of myosin isoforms. We prepared R694N, E45Q, I303V:I313V,and D208Q:K450L mutants in the β-isoform background to destabilize electrostatic interactions in the proposed regions of the myosin head. We recombinantly expressed Wild type (WT) and the mutants of the human cardiac myosin head construct (1-843 amino acid residues) in differentiated C_2C_{12} cells. Using the transient kinetics assays, we measured the kinetics of ADP release from actomyosin in the WT and mutant constructs of human cardiac myosin β-isoform. Mutant R694N showed faster rate of ADP release from actomyosin, compared to the wild type and other mutants, thus confirming that electrostatic interactions within the force-generating region of human cardiac myosin regulate ADP release and the duration of the strongly bound state of actomyosin.

DEDICATION

To all intelligent people on this planet.....

ACKNOWLEDGEMENTS

First of all, I want to thank my advisor, Dr. Yuri Nesmelov. I am so grateful to have had the opportunity to be in your lab and learn from your experience. I deeply appreciate your support throughout this extraordinary journey. I was lucky to have an incredible mentor and a humble human being as my advisor.

I thank my thesis committee, Dr. Jerry Troutman, Dr. Valery Grdzelishvili, Dr. Andrew Truman, and Dr. Kausik chakrabarti. They always encouraged me to keep my focus on solving the important problems. I learned a great deal from your lectures and about communicating my science and working through challenges. You have all been immensely supportive to me at various times when I really needed it.

I would also like to thank other faculty in the Biology department, Dr. Adam Reitzel and Dr. Richard Chi whose advice about science and other matters was invaluable to me in completing this journey.

I thank the support from Department of Biological sciences and Department of Physics and Optical Sciences at UNCC for providing me a conducive environment to learn and grow as a scientist.

The wonderful community in Dr. Nesmelov's lab made me feel immensely welcome from the very beginning. Dr. Irina Nesmelova, Dr. Jinghua Ge, Khanh Nguyen, Alexandra Hurst, Venkatesh Ranjan, Alex Grdzelishvili, Gage Leighton, Chenbo Yan and Shiril Bharadwaj have all been incredibly helpful in helping me get over the finish line, and in making our lab a great place to come to work. In terms of lab alumni, I want to specifically thank Dr. Jinghua Ge, who was a very patient and accessible mentor during our time working together.

My classmates Uday and Hyunjae have also been a great group to come through this program with. I will always remember the good times we spent together on and off campus. Finally, I want to thank my family and friends Varun, Rahul, Raghu Ram, and

Kireeti for backing me through my thick and thin; and making this journey memorable.

TABLE OF CONTENTS

LIST OF TABLES

LIST OF FIGURES

LIST OF ABBREVIATIONS

ADP Adenosine Di-Phosphate

AM Actomyosin

ATP Adenosine Tri-Phosphate

CM Cardiomyopathy

ELC Essential Light Chain

EM Electron Microscopy

HC Human Cardiac Myosin

HF Heart Failure

HLH Helix-Loop-Helix motif

HMM Heavy Mero Myosin

Pi Mono-Phosphate

RLC Regulatory Light Chain

S1 Sub fragment-1

S2 Sub fragment-2

SD1 Sub-domain 1

SD2 Sub-domain 2

SW1 Switch I

SW2 Switch II

CHAPTER 1: INTRODUCTION AND BACKGROUND

1.1 Overview of Myosin Protein

Myosin is a nano-scale motor protein that interacts with actin and ATP; transduces chemical energy into mechanical work. Multiple molecules of myosin form thick filaments in sarcomeres of muscle cells. Thick filament-forming myosin proteins are found in virtually every muscle cell: skeletal, smooth, and cardiac cells. Myosins are a superfamily of genes; ubiquitous and perform a wide range of motile functions in eukaryotes from cargo transport to cell division. Force production is ATP-dependent, myosin hydrolyzes ATP into mono-phosphate and ADP to generate power for force transduction. Myosin is conferred with an inherent ATPase enzymatic activity. Myosin motors are responsible for muscle contraction based on actin motility. Although, myosins are present in muscle cells, " unconventional myosins", that carry cargo and walk on actin filaments, with ATPase activity were first discovered in *Acanthamoeba castellanii* [1, 2]. The kinetics vary with different classes of myosin. Evolution has shaped different myosins to adapt a divergent processing speed and force generation to perform a myriad of functions from cell division to muscle contraction. A list of myosin classes and associated functions is listed in Table1.1. Over 35 classes of myosin isoforms were discovered in genomics studies [3]. All members of the myosin superfamily share several key features - namely, ATP hydrolysis enzymatic activity, actin-binding, and force generation [4].

Table 1.1: Myosin classes and functions.

Myosin Class	Functions
I	Adaptation response in the inner ear[5]
II	Muscle contraction
III	Photo transduction
V	Cargo transportation [6]
V	Endocytic vesicular transportation [7]
VI	Phagocytosis [8]
VII	Plant specific cell division [9]
VIII	Regulation of cytoplasmic flow between the cells [10] Localization of vesicles to the phragmoplast [11] Plant specific cell division [9]
IX	Single headed motor protein
X	Walks on actin bundles rather than single filaments [12]
XIV	Involved in cell invasion process [13]

1.2 Cross-bridge model of ATPase cycle

Cardiac myosin is responsible for heart muscle contraction in all animals. Figure1.1 depicts the "cross-bridge cycle" of ATP hydrolysis by actomyosin [14]. Numerous myosin molecules in the sarcomere, participate in muscle contraction using the energy generated from ATP hydrolysis. ATPase cycle follows the steps: i) Rigor state of myosin where myosin is strongly bound to the filamentous actin (F-actin), ii) Binding of ATP molecule on the ATP-binding site of S1 domain release myosin from actin, iii) Hydrolysis of ATP on the catalytic motor domain into ADP and mono-phosphate (Pi) followed by priming the lever arm, (iv) Attachment of motor domain with ADP and Pi in the ATP binding domain, to actin; weak to strong interaction transition between actin and myosin motor domain; and finally initiating actin filament sliding by lever arm rotation known as power stroke, followed by Pi release, (v) Release of ADP molecule and attain rigor state in step (i).

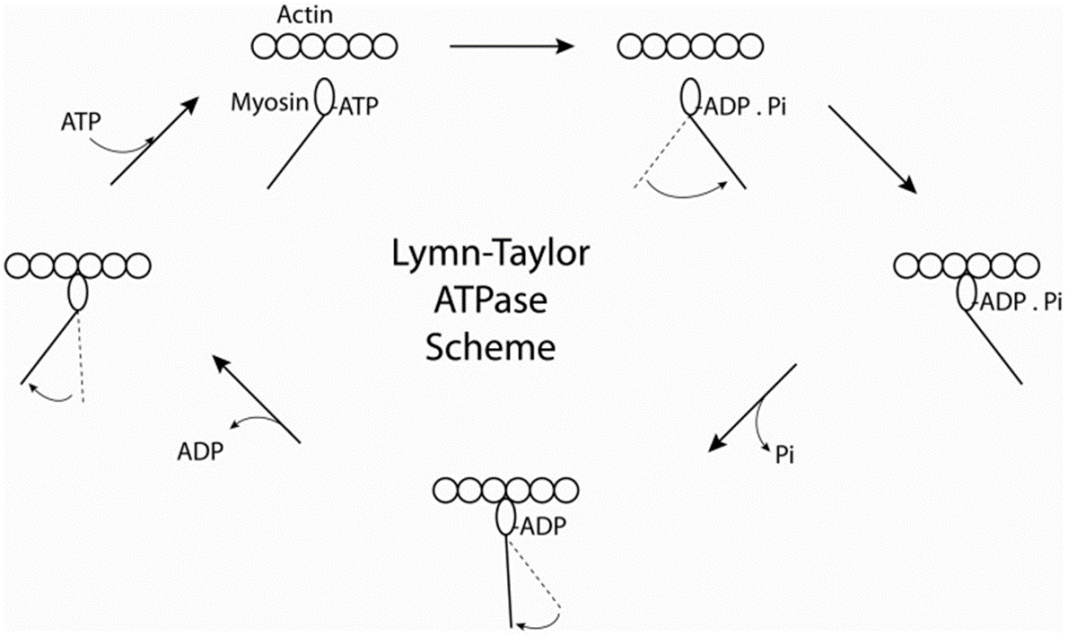

Figure 1.1: ATPase cycle of myosin

1.3 Structure of Actomyosin

Crystal structures and EM images of actomyosin and actomyosin.nucleotide complexes helped propose detailed molecular mechanisms of actomyosin interaction (Figure 1.2). High resolution EM images [15] assisted molecular dynamic simulations to generate the plausible models of structural transition states of actomyosin complex in the ATPase cycle[16, 17, 18]. The temporal order of strong to weak actomyosin transition, detachment of S1.ADP.Pi, Pi release, and ADP release from S1 are strongly debated. Some schematics show all these events in one single step to avoid confusion and display a lack of experimental evidence for these events. The experimental evidence is hard to generate is partly because of the short-lived lifetimes of these states. Unstable mechanical forces and technological advances also contribute to the lack of knowledge. Three-dimensional reconstructions of cryo-electron microscopic images of myosin head domain decorated with actin filaments revealed actomyosin interactions in distinct conformations. Helix-loop-helix (HLH) motif and surface loops on myosin interact with actin [19]. Surface loops namely- Cardiomyopathy loop (CM loop, (Figure 1.3), loop 2 (Figure 1.4), loop 3 (Figure 1.4), loop 4 (Figure 1.3), and activation loop) on myosin S1 are identified to interact with actin at the interface of actomyosin[15, 20]. Surface loops and HLH motif of myosin interact with subdomain 1 (SD1) of one actin subunit and subdomain (SD2) of adjacent actin subunit[21]. Site-directed mutagenesis of myosin surface loops coupled with actin-activated ATPase and in vitro motility studies discovered their role in actin interaction and actin-activated nucleotide release from myosin S1. Interactions with the surface loops and actin transmit conformational changes along with lower and upper 50K sub-domains of myosin head domain. The Cardiomyopathy loop (CM loop, residues 401-411 of HC β-isoform), has a conserved arginine (Arg) residue. Mutation of the conserved Arg residue on β-isoform is related to familial hypertrophic cardiomyopathy pathophysiologic condition. Point mutations on R397 of β-isoform are correlated

to cardiomyopathy in humans. Besides, numerous disease-causing mutations are found on the CM loop, underscoring its role in the actomyosin interaction of human cardiac myosin. A conserved proline-rich, actin-binding domain called "activation loop" that interacts with the N-terminal of actin, is responsible for the conformational changes rippled across β-isoform when interacted with actin. The activation loop is located on the upper helix of the relay region, which is linked to converter and lever arm regions. Activation loop is connected to the switch II (interacts with nucleotide) via the relay helix and central 7-stranded β-sheet [18, 22]. Interaction of myosin's activation loop with actin propels a conformational change across the head domain via converter domain-lever arm-relay helix-nucleotide binding site. The effect of ensemble myosin heads' activation loops with actin, eventually generates a force in muscle. 50-20K surface loop of β-isoform, referred to as "loop 2" is found at the actin-binding site. Several studies on the role of loop-2 on interaction with actin showed that it is essential for initial interaction and binding with F-actin [23, 24, 25]. The HLH motif is located in the lower 50K of β-isoform plays an essential role in the weak to the strong binding transition of actomyosin. The HLH motif along with other surface loops interacting with F-actin is part of the communication network between actomyosin interface-nucleotide binding site on myosin-relay helix-converter domain-lever arm domain.

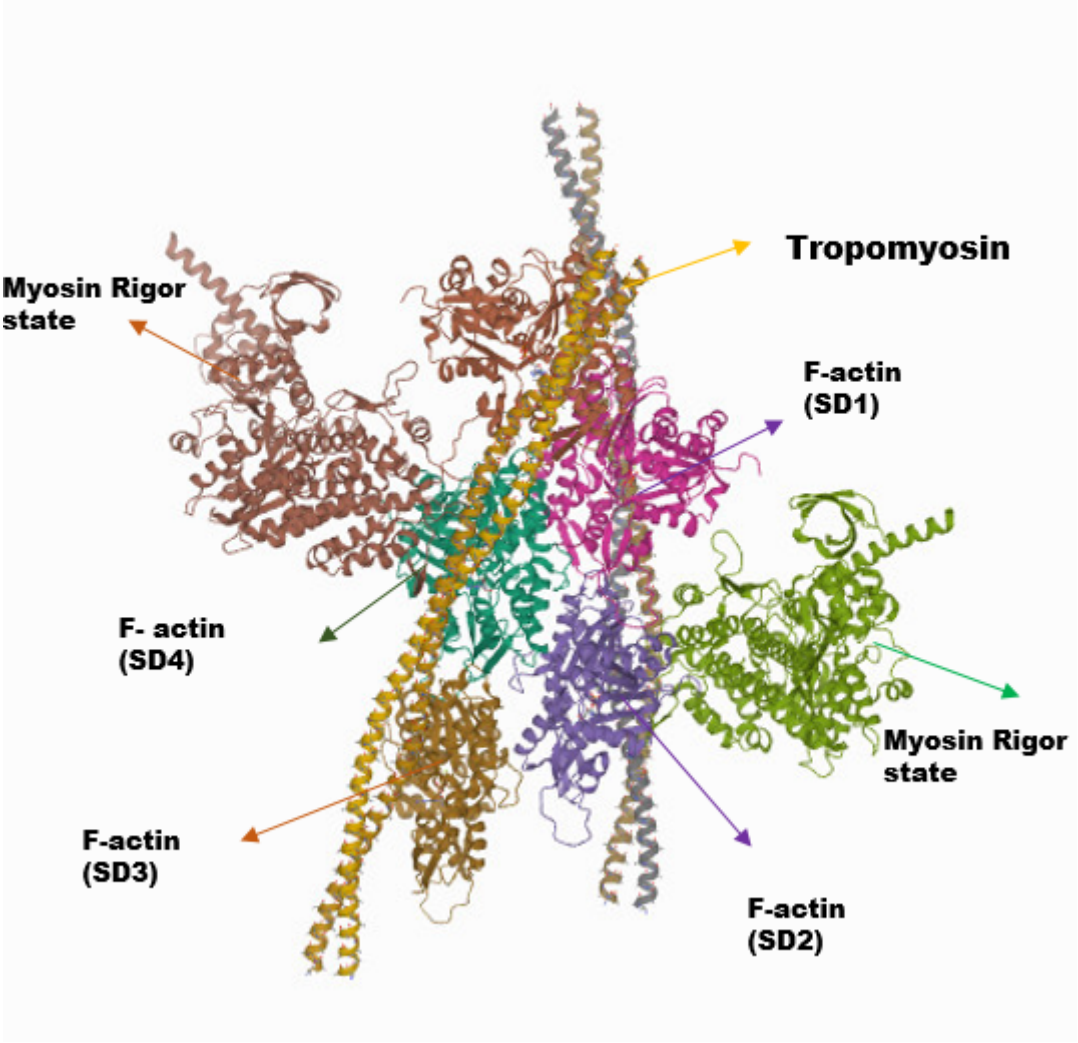

Figure 1.2: Cryo-EM reconstruction of human cytoplasmic actomyosin complex

Source: [21]

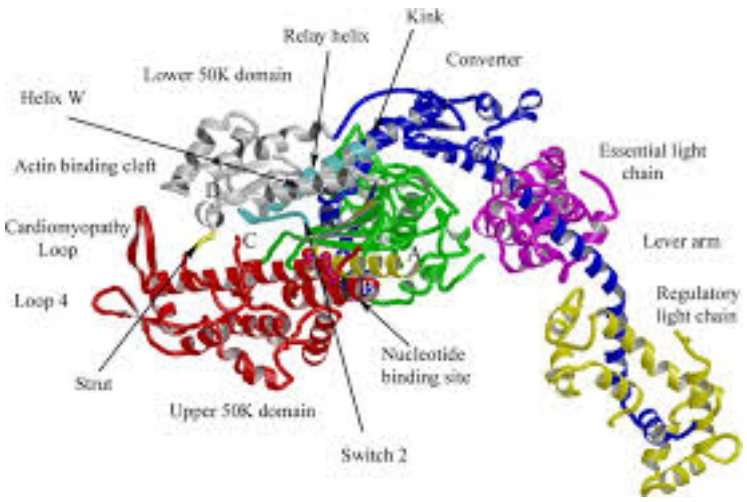

Figure 1.3: Post-Rigor structure of myosin motor domain

Source:[19]

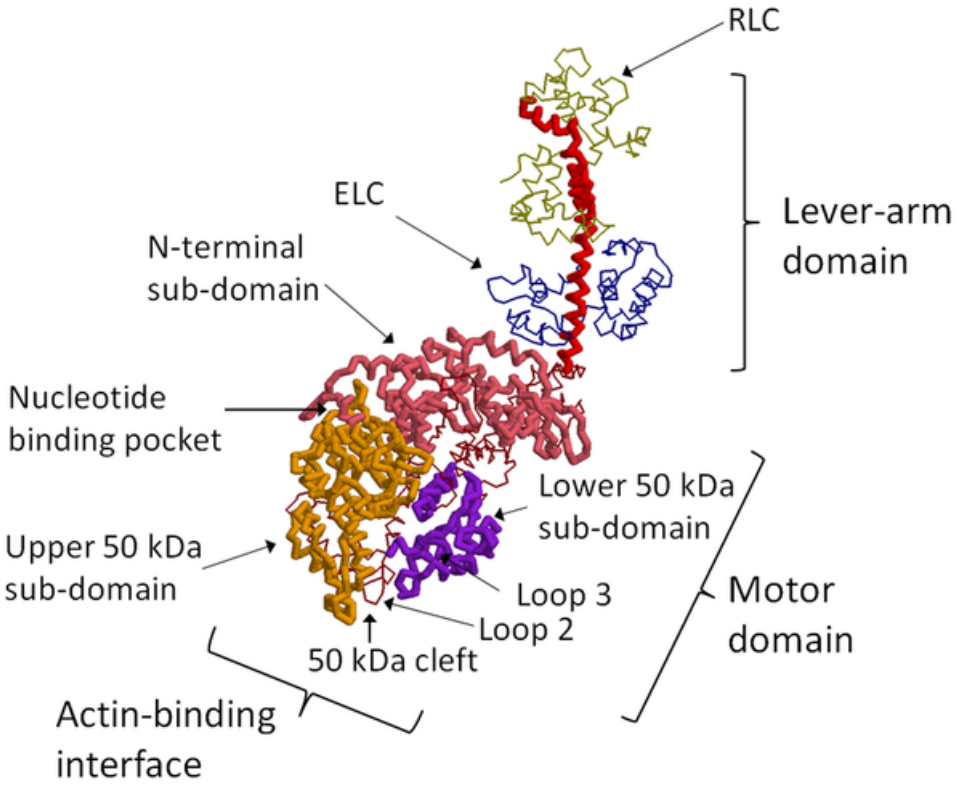

Figure 1.4: Structure of myosin II fitted based on EM data

Source:[26]

1.4 Structure of muscle myosin S1

The ATPase cycle underlies dynamic conformational changes of myosin S1 in every step. The whole process is orchestrated by communication between ATP binding site, actin-binding site, and lever arm domain of myosin. The globular head/motor domain (S1) of cardiac myosin β-isoform consists of 845 amino acids. S1 hosts the ATPase enzymatic functional domain [27]. Proteolysis studies on S1 revealed three sub structure sub-units namely - 25KDa (N-terminal), 50KDa (middle), and 20KDa (C-terminal) [28]. The 50KDa subunit is further classified into two domains called 50K upper domain and 50K lower domain (Figure 1.3). The 50K lower domain is identified as an actin-binding domain on S1 [29]. The core of the motor domain is a central 7-stranded β-sheet that contributes to all three subunits and is linked to a C-terminal tail. The N-terminal begins at the tip of the tail, first 80 residues form an SH3-β-barrel [30]. The rest of the 25K N-terminal domain coupled with 50K upper domain (residues 81-486, chicken skeletal muscle myosin [19]) forms 6 out of 7 β sheets in the core of S1. ATP-binding site is at the boundary between 25K-50K fragments, contains a characteristic P-loop that interacts with the nucleotide, found in some other ATPases [31]. Actin-binding site is a part of the lower 50k domain (residues 487-600). A positively charged loop (residues 625-647) is also identified to interact with actin. The 20K domain contains a long-running helix from the actin-binding site to the seventh strand of the β sheet. Helix is continued into a turn (SH1), a broken helix (SH2), and into a compact converter domain (residues 711-781). Converter domain functions as a linker between the C-terminal-helical tail and two light chains (ELC and RLC). This entire region is termed as "neck region" or regulatory domain of S1[32]. During the ATP hydrolysis, the neck domain amplifies the rotation movements by the converter domain.

1.5 Domains of Myosin

All myosin molecules (all classes and isoforms) are composed of head/motor, neck, and tail domains. The motor domain is also known as the catalytic domain which hosts ATP and actin-binding sites. The neck domain acts as a linker and lever arm between the tail and motor domains (Figure 1.2). Rotation of lever arm domain delivers force to the motor domain and thereby induces actin filament sliding. Amino acid sequence analysis studies revealed great variation among tail domains and motor domains between various classes of myosin in different species. Class II myosins share similar structural and functional properties. The general structure of full-length myosin II as a dimer is shown in Figure 1.5.S1 hosts motor domain and two light chains: Essential light chain (ELC) and Regulatory light chain (RLC) . The Coiled-coil tail domain is referred to as S2. Proteolysis of full-length myosin with trypsin or chymotrypsin enzyme yields two domains of S1 and S2 together, referred as Heavy Mero Myosin (HMM). The C-terminal tails from numerous myosin heads form thick filaments in the sarcomere. Myosin motor domain or S1 is obtained from chymotrypsin digestion, retains ATPase and actin-binding capability [33]. We are interested in characterizing the structure-function relationship of muscle myosin. To investigate the role of the myosin motor environment on its interaction dynamics with its ligands, we used rabbit skeletal myosin as a model system. Our goal is to understand the role of electrostatic interactions within the motor domain of human cardiac myosin β-isoform (HC-β) on its kinetic performance. Cardiovascular diseases like Hypertrophic Cardiomyopathy and Dilated Cardiomyopathy are caused due to the mutations on sarcomere proteins- tropomyosin, troponin, and predominantly human cardiac myosin β-isoform (HC-β).

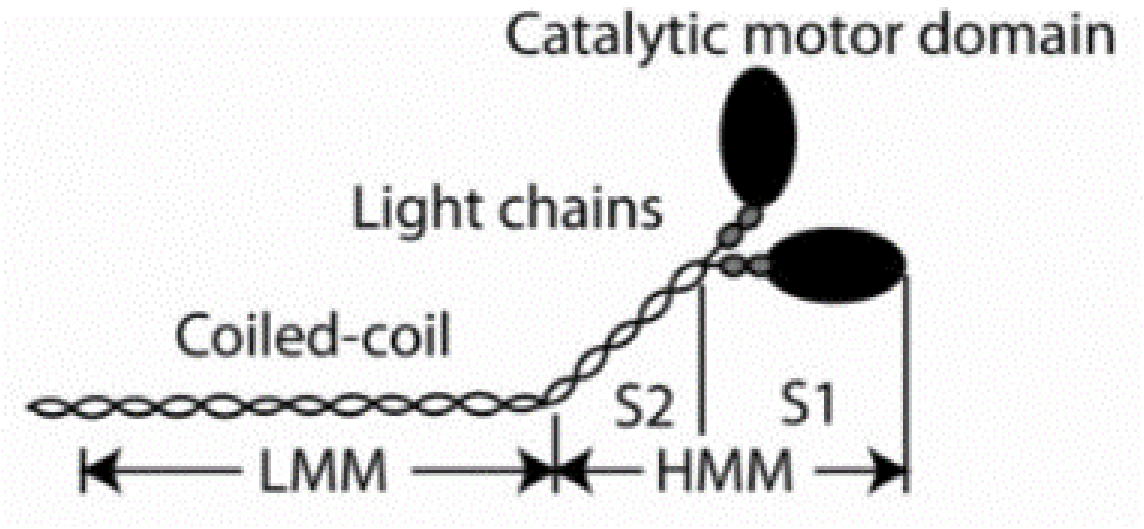

Figure 1.5: Domains of myosin

1.6 ATP interaction with myosin

The myosin ATPase cycle involves three main components of myosin. (i) The central core of myosin motor domain with 50K lower domain. P-loop which plays a key role in nucleotide interaction with myosin is a part of this domain. (ii) The upper 50K domain and switch 1 (SW1). (iii) Switch 2 (SW2), converter domain, relay loop, and the lever arm domain. The nucleotide pocket is made up of P-loop, SW1, and SW2. The ATPase cycle of myosin has been outlined 40 years ago, but the mechanism of certain intermediate steps like catalytic hydrolysis of substrate, within the cycle, remains elusive today. The nucleotide-binding site of myosin is located between upper and lower 50K domains on S1 (Figure 1.4). Mg.ATP is the physiological substrate for myosin ATPase enzymatic activity. A high concentration of Mg^{+2} inhibits the reaction rate of catalytic hydrolysis of ATP [34]. A high turnover rate of ATP hydrolysis is observed in the absence of Mg^{+2}. Following the hydrolysis of ATP, myosin undergoes a cascade of conformational changes that allows myosin to generate force and pull actin filaments. In vitro experiments on myosin S1 and ATP in the absence of F-actin filaments, show a rapid irreversible binding step of S1 to Mg.ATP and rapidly reversible hydrolysis of Mg.ATP to Mg.ADP.Pi. In the

absence of actin, Mg.ADP.Pi is tightly bound to S1. ADP release step is slow and only occurs after Pi release step. The mechanism of Mg.ADP release is elusive and varies depending on different myosin isoforms. ATP and ADP.Pi bound S1 states are well studied from the crystal structures of analogs, ADP.AlFx, ADP.BeFx, and ADP.Vi[35]. Various analogs, inhibitors, and transition state complexes made it possible to study the conformational states of S1 throughout the ATPase cycle. From a thermodynamic perspective, the binding energy of S1.ATP complex in conjunction with the hydrolysis step primes myosin to bind actin and generate force for muscle contraction.

ATP binding to actomyosin step: In the A.M rigor actomyosin state, the upper 50K domain cleft is in a closed state. This allows actin-binding 50K cleft on S1 to interact strongly with actin. With both SW1 and SW2 open, the nucleotide-binding site is open during the rigor state. ATP binding to the nucleotide site on S1 closes SW1 onto the nucleotide. This interaction triggers a rotation of the 50k domain and disrupts actomyosin interaction.

ATP hydrolysis: SW2 interaction with ATP triggers a rotation of lever arm via relay helix that connects SW2 and converter domain. S1 detaches from actin and assumes a primed-up conformation called recovery stroke. Closure of SW1 and SW2 follows ATP hydrolysis and the formation of a stable S1.ADP.Pi complex.

Actin binding and Power Stroke: After ATP hydrolysis, the affinity of S1-actin increases, the lower 50K domain interacts with actin, and the cleft between upper and lower 50K domains closes and S1 binds to actin. This interaction triggers converter domain distortion, rotation of force-generating region (SH1-SH2) helix, and generates force. Force generation provided in this step assists in actin filament sliding called power stoke. The temporal order of events of Pi release and power stroke is debated. After the power stroke, the converter domain re-organizes, opens up a nucleotide pocket to allow ADP release and a new ATPase cycle to begin [36].

Actin contact with the activation loop on S1-actin interacting surface initiates Pi re-

lease from S1.ADP.Pi complex in *Dictyostelium* myosin II[37]. It is not clear whether the Pi release occurs before or after the cleft closure and formation actomyosin complex. A popular view called "Back door mechanism" proposes that ADP blocks the exit of Pi from the nucleotide pocket of S1. Pi is thought to be escaping from the 50kDa-cleft opening. So, the release of Pi from the AMD complex depends on the cleft opening (back door)[35]. Site-directed mutational constructs of S1 that block the opening of cleft/back door, support the inhibition of Pi release, and provide some evidence for the back-door mechanistic model[38]. Alternative counter view proposes an opening of SW1 aided Pi release[34]. Pi release is linked to force generation and power stroke, and the hypothesis of Pi release from cleft before the strong actomyosin interaction raises questions against the back door exit hypothesis. Pi release during the weak interaction state of actomyosin.ADP.Pi may cause mechanical failure. FRET and optical trap experiments on myosin V show a very dynamic myosin in the absence of actin, presence of actin traps S1 in post power stroke conformation that precedes Pi release[39, 40, 41]. The mystery surrounding the Pi release step is not resolved and needs further experimentation to change the strongly-held opinions by different research groups. One surprising revelation is the reversible binding of Pi to the nucleotide-binding site and cycles back to form tightly bound ATP.S1 complex[42, 43]. The energy is dissipated only after the power stroke and irreversible release of Pi occurs[42]. The presence of load promotes the irreversible release of Pi and ADP release from M.ADP complex[34]. When compared to Pi release, the ADP release step is well studied and much better understood. ADP remains within the nucleotide pocket of S1 until the power stroke step is complete.

1.7 Role of SW1 and SW2 in ATP hydrolysis

Crystal structures of myosin with ATP and ADP.Pi analogs revealed the significance of two loops (SW1 and SW2) with ATP interaction and hydrolysis. The nucleotide-binding site is mainly formed by a make-shift cleft created by SW1, SW2, and P-loop.

Rapid kinetic studies combined with crystal structures provided contemporary transition state conformations of myosin.nucleotide interaction. Based on these studies, on a wide range of myosin types, molecular dynamic simulations[44, 45], the ATPase mechanism is proposed to follow the listed steps. Mg.ATP interacts with the nucleotide pocket on S1 by three loops (SW1, SW2, and P-loop), the γ-Pi of ATP is stabilized by the H-bonds peptide interaction[44, 46] with the P-loop. Crystal structures of *Dictyostelium* myosin II, with Mg.ADP.Vanadate, that supposedly mimics, S1.ADP.Pi interaction shows a stable interaction of Mg.γ -Pi group with P-loop. SW2 forms a salt-bridge with SW1 to stabilize SW1 interaction with Mg^{+2}[44]. ATP hydrolysis is proposed to be catalyzed by the Glu459 residue on SW2. Glu459 residue on SW2 forms a salt bridge interaction with Arg238 on SW1. Glu459 participates in proton transfer reaction from the two water molecules found in the nucleotide-binding site of S1. Based on computational molecular dynamics simulations, Glu459 is hypothesized to transfer proton from water molecule to the γ-Pi of the Mg.ATP[44, 47]. Following the proton transfer, a meta-phosphate is created by breaking the β-Pi bond between the γ-Pi and bridging oxygen atom. P-loop, SW1, and SW2 stabilize this interaction and support the formation of an intermediate metaphosphate group. The steps involved in the ATPase catalytic mechanism are being debated for over 20 years, and the most accepted model of mechanism is presented here, needs further experimental verification.

1.8 Theoretical Understanding behind ATPase cycle mechanism

The model mechanism of actomyosin interaction with ATP is built on kinetic experimentation that satisfies the fundamental thermodynamic laws of nature. Binding and hydrolysis energy associated with ATP interaction with S1 and ATP hydrolysis step, dictate the efficiency and timing of the events in the ATPase cycle. Actin, in rigor state has a very high affinity to myosin (K_d *approx* 10nM)[34]. The binding of ATP to the nucleotide-binding site on myosin S1 displaces actin from myosin. This association

promotes the opening and closing of the nucleotide-binding pocket mediated by SW1. Recovery stroke and γ-Pi stabilization within the pocket with SW1, SW2, and P-loop interaction follow. Reversible interactions of the Pi group on ATP with amino acids on nucleotide pocket loops are associated with small free energy changes. The free energy change associated with the first conformational change of myosin, that is actomyosin dissociation step and recovery stroke is provided by the binding energy of ATP interaction with S1. The hydrolysis step is reversible [48], the degree of reversibility governs actomyosin interaction dynamics. The rate of ATP hydrolysis step drives the whole ATPase cycle forward and partially dictates the turnover rate of each myosin motor. Actin plays a key role in the lifetime of S1-ATP interaction. In the presence of actin, S1 motors exhibit a very high turnover rate[49]. The regulation of turnover rate by the lifetime of S1-ATP interaction of a single ATPase cycle is quantified by a parameter called "*DutyRatio*"(DR). The energy associated with ATP hydrolysis, is translated into a working power stroke, only then, Pi interaction with S1.ADP becomes irreversible. The details of how the energy is used by the S1 molecule are not clearly understood. It could be vibration energy between the atoms of the S1 molecule, or elastic-mechanical transduction by bending or stretching of S1. Mechanical coupling of the central β-sheet and lever-arm domains play a role in chemical to mechanical energy transduction. In a muscle cell, tiny contractile units-sarcomeres contract by the motion of millions of myosin heads. Load-dependent mechanical stress on several myosin heads results in sarcomere shortening. How individual motors share load-bearing conformational behavior compared to single motors without any load needs further investigation. ADP release step is the most divergent step, in terms of thermodynamic perspective that varies in different classes of myosin[50]. The rate of ADP release dictates the free energy change associated with a specific myosin. A faster ADP release rate, involves a significant negative free energy change [34], whereas, a slow ADP release, is associated with a zero-minimal free energy change. Motors with a fast ADP release characteristic, generate a fast movement

of the motor under load, for example, fast skeletal muscle myosin. Motors with a slow ADP release characteristic, generate a slow and long-lasting force on the actin filaments, for example, smooth muscle myosin. The rate of ADP release is encoded within the gene of a particular myosin. HC β-isoform is coded by gene MYH7, show a slow ADP release rate. ADP release with a positive free energy change is not observed in myosin II, but observed in processive motors, such as myosin V [51].

1.9 Role of Human cardiac myosin isoforms in pathophysiology of Heart Failure

Heart failure is one of the cardiovascular diseases that is affecting millions of people in the USA and worldwide. A recent statistic from American Heart Association (AHA) predicts a dramatic increase of HF patients by 46 percent by 2030[52]. Weakened cardiac performance is a major hallmark of HF. Power output decline is improved by loading heart muscle with inotropic agents and Ca^{+2} ions. Excess Ca^{+2} inside the cytoplasm increases the actomyosin interactions, as a result, excess myosin heads are activated. This leads to excess consumption of oxygen, which eventually leads to ischemic and arrhythmic conditions in the heart. Recently, a new paradigm of drugs Omecamtiv Mecarbil (OM), Mavacamten, and Levosimendan shown to regulate proteins on a sarcomere level. Levosimendan sensitizes thin filaments, OM and Mavacamten directly act on cardiac myosin motors and thereby increase the efficiency of the heart. Nevertheless, the potential side effects that cause arrhythmias are still under investigation. Novel therapeutic approaches are required to improve cardiac performance without causing side effects. In this study, we are looking for regulatory sites in cardiac myosin to regulate the myosin performance at existing Ca^{+2} levels. In the left ventricle of the human heart, cardiac myocytes express two myosin isoforms α isoform (10% composition, kinetically fast) and β isoform (90% composition, kinetically slow), homogeneously distributed[53, 54, 55, 56, 57, 58]. A decline in α isoform content is a sign of a decrease in power output of the muscle [59]. Increased α isoform count inferred cardioprotec-

tion in rat and rabbit animal models [60, 58]. Discovering the underlying differences between both the isoforms will potentially lead to drug target sites that can improve the performance of a failing heart.

1.10 Structural differences between isoforms of Human cardiac myosin

Our analysis on amino acid sequences of α and β isoforms revealed 80 differences between them. They share a 93 % sequence similarity. ADP release from actomyosin is an order of magnitude faster in the alpha myosin isoform [61]. Small differences in the sequence are responsible for distinct local inter-residue interactions within α and β isoforms, leading to a dramatic difference in the rate of ADP release. Our analysis of structural kinetics of α and β isoforms using molecular dynamics simulations revealed distinct dynamics within the force-generation region of the myosin head. The simulations identified some permanent salt bridges in the β-isoform, which are not present in the α-isoform [62]. These isoform-specific electrostatic interactions might play a role in the difference in kinetic properties of myosin isoforms. In this section, apparent structural differences in the motor domain of both isoforms are discussed.

1.10.1 Structural Variation of Loop 1

Loop 1 is a flexible surface loop, part of the transducer region, is located near the nucleotide-binding site on the myosin motor domain. Loop 1, also known as 25/50-kDa loop is located near the active site on S1. Loop 1 is believed to be involved in the actin-activated ATPase function of myosin. Loop 1 is one of the major determinants in the kinetic tuning of various motors in the myosin II family [63]. Single-molecule studies show regulation of force and velocity of actin filament sliding is governed by predominantly two surface loops (loop 1 and 2) on the myosin motor domain. Loop 1 studies of myosin II have shown its effect on actomyosin interaction with ADP [63, 64, 65, 66, 67]. Truncated loop 1 studies on mammalian myosin I (MyoIb), have shown to affect, actomyosin affinity to ATP binding, actin-myosin Ib affinity, ADP release from

actomyosin, and actin dissociation from MyoIb [68]. Similar studies carried out on MyoIc which functions as an adaptation motor in the hair cells of the inner ear show that loop 1 affects nucleotide-binding properties of MyoIc [69]. Alternative splicing within the myosin II family gene sequence generates a range of splice variants with varying loop 1 lengths and sequences. Force measured by micro-cantilevers on myosin II of mollusk, skeletal, and smooth muscle filaments, discovered a close correlation between loop 1 sequence, length on the sliding velocity of thin filaments [70]. Studies carried out by cleavage of loops 1 and 2 on skeletal muscle HMM, report a decreased ATPase activity and lower load-dependent actin sliding velocity [71]. Chimera construct studies on loop 1 derived from various myosins including α and β isoforms show that the sequence of loop 1 affects the rate of ADP release [72, 66, 73, 74]. The majority of loop 1 studies were carried out on *Dictyostelium* myosin but not on cardiac myosin. Figure 1.6. shows the structural differences within loop 1 region between both isoforms. Different sequences produce structural differences. Loop1 in α myosin more helical, that effectively decreases loop1 length and removes the loop1 7-stranded β sheet interaction. R204:E217(218) is the permanent salt bridge, maintaining Loop1 structure. Residues 198:216 of Loop1 gain helical content in α myosin (Figure 1.6, right), due to the sequence difference in its flanking residues. As the result of this, Loop1 in β myosin does not maintain the contact with the central 7-stranded β sheet via the salt bridge D208:K451 (α isoform sequence, D208:K450 in β myosin), as in β myosin (Figure 1.6, left). Loop1 in α myosin is shorter, differently oriented, and loop1 is connected to the nucleotide-binding site (P-loop and loop Switch1) via two flanking helices. Uncoupling of loop1 and 7-stranded β sheet might affect myosin-nucleotide interaction and may modulate the rate of ATP hydrolysis and ADP release. The modulation of time when the bridge is ON may regulate the mechanism of myosin kinetics, residues D and K, which are conserved across different myosins may play a part in this regulation. Then, the modulation should depend on the loop1 sequence and length, as was proposed before [75, 72]. Another salt bridge

within the loop1, R204:E218 in β myosin, R204:E217 in β myosin, is in both isoforms, preserves Loop1 structure (Figure 1.6). The uncoupling of the R204:E217 bridge in β myosin may have the same effect as uncoupling of D208:K450 and potentially modulate β myosin kinetics, due to resulting increased flexibility of loop1.

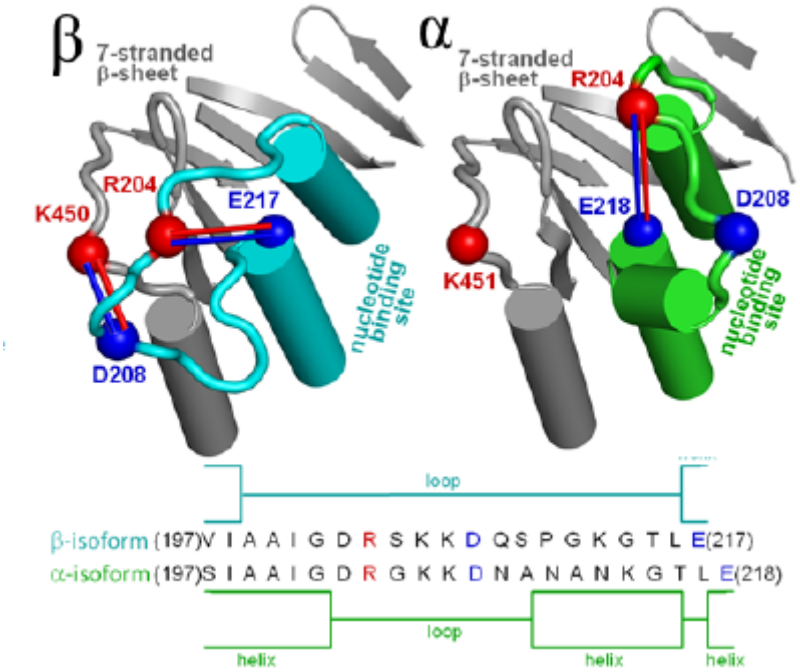

Figure 1.6: Variation of Loop 1 in cardiac myosin isoforms

*Loop1 (left, cyan, β myosin, and right, green, α myosin) and the 7-stranded β sheet (gray) are coupled in β myosin and uncoupled in α myosin.

*Red and blue spheres are the positive and negative charged residues. Red-blue sticks represent the salt bridges.

*The uncoupling of the R204:E217 bridge in β myosin may have the same effect as uncoupling of D208:K450 and potentially modulate β myosin kinetics, due to resulting increased flexibility of loop1.

1.10.2 Structural Variation in Loop I289-D324

Figure 1.7. shows the structural differences within loop I289-D324 region between both isoforms. Loop I289-D324, structurally different in α and β isoforms is located near the loop Switch1 of the active site. During our MD simulation, the loop I289-S314 gains helical content (residues N306-S314) and becomes more flexible in the β isoform compared to α isoform. Two residues, V304 and V314 in α isoform are replaced with I303 and I313 in β isoform, affect the loop I289-D324 conformation. Structural analysis in β isoform shows that I303, I313, and L290 form a leucine-isoleucine zipper, apparently stabilizes the helix N306-S314 and as a result changes the loop I289- D324 conformation. Different interaction between two loops in α and β isoforms is indicated by the isoform-specific salt bridge E317:K234 (populated 38.7% in α isoform and only 2.4% in βisoform), and probably stabilizes the loop I289-D324 and loop Switch1 interaction in α isoforms. Such interaction between loops may modulate loop Switch1 structural dynamics and therefore, myosin-nucleotide interaction.

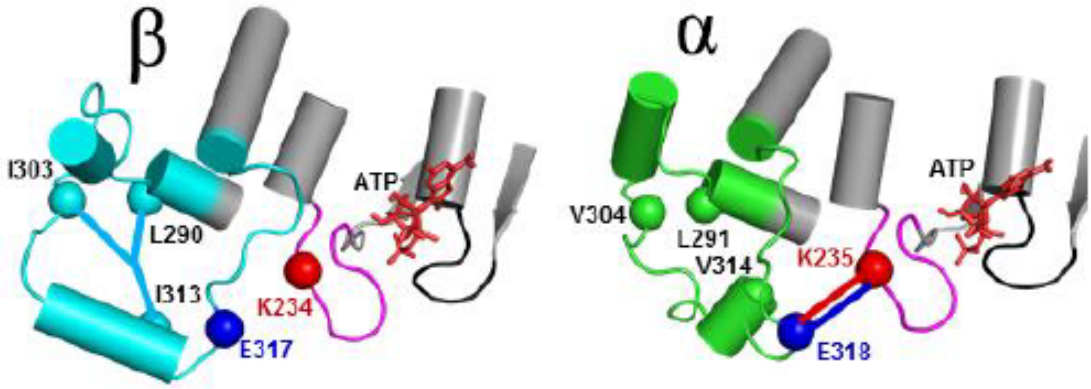

Figure 1.7: Variation of Loop I289-D324 in cardiac myosin isoforms

*The loop I289-D324 and the loops of the active site (magenta, loop Switch1, black, P-loop).

*Red sticks, ATP. Red and blue are the positive and negative charged residues.

*Left, β isoform, leucine-isoleucine zipper (I303:L290:I313, cyan sticks) configures the loop I289-D324 for smaller interaction with the loop Switch1, as indicated by the absence of the salt bridge K234:E317.

*Right, α isoform, the loop I289-D324 has no zipper (Ile-Val sequence replacement), and the stable salt bridge K235:E318 forms (red-blue sticks), indicating the loop I289-D324 and loop Switch1 interaction.

1.10.3 Structural Variation in SH1-SH2 helix region

Figure 1.8. shows the structural differences within the SH1-SH2 helix region between both isoforms. Position of N-terminal domain β barrel (gray) relative SH2 and SH1 helices modulates electrostatic network in the region and thus affects the stability of SH1 helix. SH1 helix is properly folded in α myosin and unwound in β myosin. We conclude that the relative position of the N-terminal domain plays a significant role in these isoform-specific electrostatic interactions. The N-terminal domain shows about 17% sequence difference in α and β myosin. The different relative position of N-terminus and SH1-SH2 helices is due to this sequence difference. SH1 helix instability in β myosin is affected by this structural difference, affects local electrostatic interactions, and thereby affecting myosin kinetics. Unwound SH1 helix was observed in the crystal structure of scallop striated muscle myosin, complexed with ADP [76], and it was proposed that SH1 helix melts during myosin ATPase cycle [77]. How this melting affects myosin structural kinetics is not known.

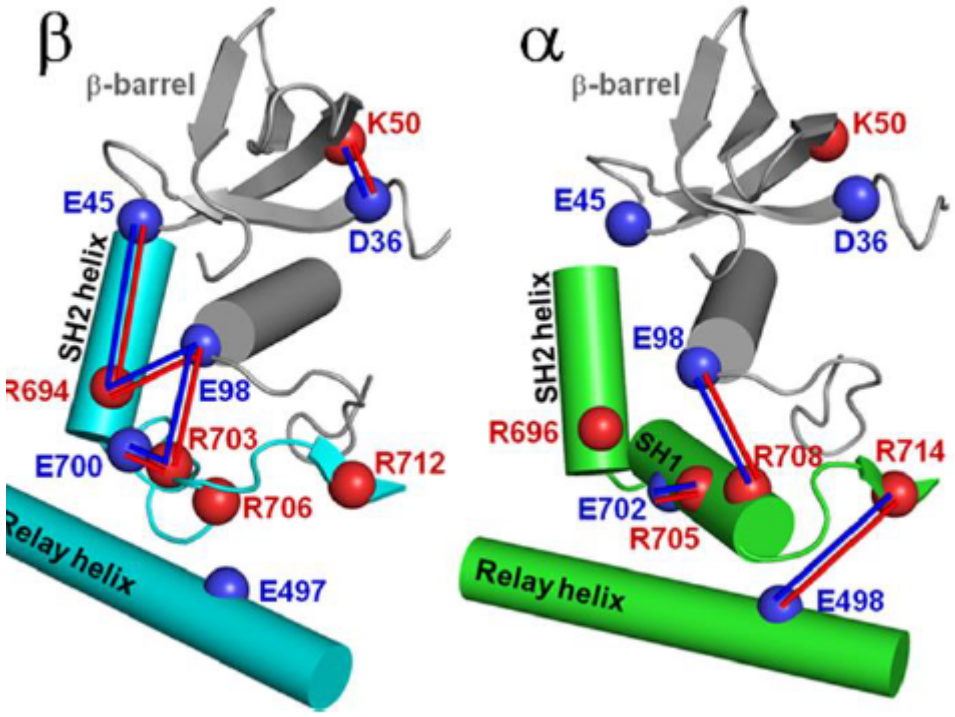

Figure 1.8: Structural Variation in SH1-SH2 helix region in cardiac myosin isoforms

*Myosin force generation region, β (left panel) and α (right panel) isoforms.

*Red and blue are the positive and negative charged residues. Red-blue sticks represent the salt bridges.

*Mutation affecting the SH1-SH2 helix region on β-isoform: Two β-isoform mutations, R694N and E45Q potentially affect the electrostatic network within SH1-SH2 helix region, which is connected to the SW2 via relay helix.

1.11 Choice of mutations and myosin regulation

Based on the MD simulations, we obtained three potential sites within the motor domain of human cardiac myosin β-isoform, that might potentially affect actomyosin cross-bridge kinetics. Our focus is on understanding how these sites regulate actomyosin interaction with the nucleotide and the rate-limiting step (ADP release) [61] kinetics in the ATPase cycle. The nucleotide-binding site on myosin is mainly composed of three highly conserved loops: P-loop (residues 177-184, α cardiac myosin sequence), Loop switch I (SW1, residues 232-246), and Loop Switch (SW2, residues 462-474). Site-directed mutagenesis studies on these loops of myosin II, severely affected the nucleotide-binding and ATPase activity of myosin [78, 79, 80, 81, 82, 83, 84, 85]. Therefore, we chose to modulate the interaction of actomyosin-nucleotide, indirectly by changing the conformation and the dynamics of the nucleotide interacting loops.

A mutation affecting Loop 1 conformation on β-isoform: Loop 1 and the β-sheet are permanently coupled in β-isoform (Figure 1.6) and completely uncoupled in α-isoform. We proposed a double mutation at D208Q: K450L in β-isoform. Mutation D208Q: K450L will potentially uncouple loop1 and the β-sheet, producing α-myosin-like interaction of loop1 and the β-sheet. This isoform-specific mutation will potentially affect the affinity of nucleotide to actomyosin.

A mutation affecting the interaction of Loop Switch I and loop I289-D324 on β-isoform: The double mutation, I303V: I313V, potentially mimics, α-isoform version of the loop I289-D324 in β-isoform (Figure1.7). This mutation may break the leucine-isoleucine zipper and promote the loops coupling in β isoform. Such interaction might modulate the loop Switch 1 structural dynamics, affecting myosin nucleotide interaction, and regulating the kinetics of cardiac myosin.

A mutation affecting the SH1-SH2 helix region on β-isoform: Two β-isoform mutations, R694N and E45Q potentially affect the electrostatic network within the SH1-SH2

helix region, which is connected to the SW2 via relay helix. Mutation R694N disrupts two stable salt bridges, R694:E45 and R694:E98. Due to the high sequence conservation of SH1 and SH2 helices among myosins, mutagenesis of R694 might be a too strong perturbation. We, therefore, chose a milder mutation E45Q within N-terminus. Both proposed mutations are meant to break the R694:E45 salt bridge and thus redistribute electrostatic interactions within the force-generating region in β- isoform (Figure 1.7).

1.12 Role of CaATP in regulation of myosin

Muscle contraction relies on Calcium concentration within the muscle cells. Thin filament proteins, troponin, tropomyosin, and actin, interact with calcium ions to regulate sarcomere contraction. Calcium-binding to troponin induces a conformational change in thin filaments that exposes actin-binding sites to myosin heads in thick filaments. Calcium released from sarcoplasm reticulum, enters the z-line of sarcomere [86]. Diffusion-mediated transport delivers calcium ions to thin filament proteins. ATP in the muscle cells can bind to calcium and magnesium ions depending on their respective temporal concentration changes. Calcium concentration in the sarcoplasm varies in response to transient waveforms [87]. MgATP is the primary ligand for myosin ATPase enzymatic activity. Even at high magnesium concentrations, some myosin heads inevitably bind to CaATP molecules. Therefore, it is important to understand the role of CaATP in regulating actomyosin kinetics within skeletal and cardiac muscle tissues. Our studies on CaATP-actomyosin interactions attempted to answer several open questions on CaATP-induced actomyosin dissociation and CaADP release from myosin. We chose rabbit skeletal muscle myosin as a model system to investigate the molecular mechanisms of the ATPase cycle with CaATP as a primary ligand. We performed steady-state actin-activated myosin ATPase assay and basal myosin ATPase assay with CaATP and MgATP as ligands, to quantify the duration of the whole actomyosin cross-bridge cycle. Pathological conditions like malignant hyperthermia are associated with high calcium

influx in sarcomere of the skeletal muscle cells [88]. At elevated concentrations of calcium in the sarcomere, more myosin heads bind to CaATP that consequentially causes muscle rigidity observed in skeletal muscle cells [89, 90].

1.13 Role of macro molecular crowding in regulating myosin kinetics

Structural, functional, and kinetic studies of myosin, carried out in diluted solution environments, do not accurately model the behavior of the motor. The cellular environment is much crowded relative to reconstituted experimental conditions in vitro. The diffusion rate of macro-molecules, small molecules, and ligands vary with the surrounding chemical environment. The functioning of enzymes in crowded environments is constrained by steric hindrance and unusual non-specific molecular interactions[91]. Understanding of myosin function in a crowded environment depends on the type of crowding agent and concentration of the agent. Modeling of the crowding environment plays a key role in interpreting the effects of crowding agents on the kinetics of myosin. A popular model for interpreting crowding effects is the excluded-volume model, where crowding agents are modeled as hard-repulsive spheres. In the excluded-volume model, the space between molecules is reduced with an increase in the apparent concentration of solute or other small molecular ligands. Ficoll-70 is a typical macro-molecular crowding agent used to study protein stability, conformation, the entropy of unfolding, and preference over native or compact states [92]. We chose rabbit skeletal muscle myosin II as a model system to investigate the molecular mechanisms of the ATPase cycle in a crowded environment with Ficoll-70 as a crowding agent. We performed basal myosin ATPase assay, ATP-induced actomyosin dissociation assay, and ADP inhibition of ATP-induced actomyosin dissociation assay with Ficoll-70 as a crowding agent. Based on biochemical and biophysical assays, excluded-volume model, and diffusion studies on F-actin and ATP in Ficoll-70, we conclude that functional model of actomyosin-nucleotide interaction is affected by crowded micro environment.

1.14 Synopsis

Myosin regulation has a long and storied history. In this introductory chapter, the roots of this field were traced back to scientific observations made on the molecular basis behind the muscle contraction and myosin ATPase cycle. However, the individual steps employed by myosin during the ATPase cycle, are not completely resolved to date. While the idea of regulation of cardiac muscle contraction by targeting sarcomere-proteins has been tried several times, the numerous cellular players involved in the process made the regulation challenging. Our understanding of the structure-function relation of a major player in cardiac muscle contraction–Human cardiac myosin motor protein, has the potential to enable the clinical application of increasingly sophisticated muscle regulation strategies.

The complex, multi-step process of ATP hydrolysis by myosin were described in detail in this introductory chapter. Our strategies to regulate cardiac myosin by altering its intramolecular electrostatic interactions, furthered the understanding of cardiac myosin kinetics. Chapter 2 will describe the generation of novel recombinant human cardiac myosin head domain (β-isoform) constructs. Chapter 3 will describe extensive kinetic characterization of these constructs uncovered unexpected roles of intramolecular electrostatic interactions for regulating cardiac myosin function. Chapter 4 will discuss relevance of these results in the broader context of myosin regulation, and concludes with a perspective on the promise of myosin regulation therapy in cardiovascular diseases.

CHAPTER 2: METHODS

2.1 Protein Preparation

The β-isoform construct of human cardiac myosin motor domain contains $1-843$ residues and FLAG affinity tag at the C-terminus. Adenoviruses encoded with the wild type and R594N, E45Q, D208Q:K450L, and I303V:I313V myosin mutants were purchased from Vector Biolabs (Malvern, PA), amplified using HEK293 cells (ATCC CRL-1573), and purified using CsCl gradient centrifugation. Recombinant human cardiac myosin was expressed in C_2C_{12} (ATCC CRL-1722) mouse myoblast cells. C_2C_{12} cells were grown to a 95% confluence on 15 cm diameter plates and infected with the optimum dosage of virus determined by a viral-titration assay. Cells were allowed to differentiate post-infection and collected seven days post-infection to extract and purify myosin. Collected cells were washed and lysed in the presence of a millimolar concentration of ATP. The cell lysate was incubated with anti-FLAG magnetic beads (Sigma-Aldrich, Milwaukee, WI). Beads were washed and myosin was eluted from the beads by 3x FLAG peptide (ApexBio, Houston, TX). Myosin purity was assessed by Coomassie-stained SDS-polyacrylamide gels (Figure 2.1) and protein concentration was determined by measuring the absorbance at 280 nm using the extinction coefficient ϵ_{280nm} =93,170 $M^{-1}cm^{-1}$, calculated using the ProtParam tool of ExPASy web server.

Rabbit skeletal myosin (full-length) and actin was prepared from rabbit leg and back muscles [93]. Chymotryptic S1 was prepared as described [94], and dialyzed into experimental buffer F-actin was labeled with pyrene iodoacetamide (Life Technologies Corporation, Grand Island, NY) with the molar ratio 6:1, label:actin. After labeling, actin was cleaned from the excess of label, re-polymerized, stabilized with phalloidin at the molar

ratio of 1:1, and dialyzed for 2 days at T=4 °C against the experimental buffer. Concentration of unlabeled G-actin was determined spectrophotometrically assuming the extinction coefficient ϵ_{280nm}=0.63 $(mg/ml)^{-1}cm^1$ [95]. Concentration of labeled G-actin and labeling efficiency were determined spectroscopically using the following expressions: [G-actin]= $(A_{290nm} - (A_{344nm}.0.127))/26{,}600\ M^{-1}$ and [pyrene]=A_{344nm} /22,000 M^{-1} [96]. Pyrene labeling efficiency of actin was usually about 70%. The experimental buffer contained 20 mM MOPS (3-[N-morpholino]propanesulfonic acid) pH 7.3, 50 mM KCl, 3 mM $MgCl_2$ total concentration. Since $log_{10}K_A$ for MgATP is 4.29 [97], where K_A is the association constant, 3 mM $MgCl_2$ chelated all ATP used in our experiments, since used ATP concentration was 0.9 mM or less. We do not expect any measurable effect from the K_{ATP} complex since the association constant for such a complex is three orders of magnitude smaller than the constant for MgATP and CaATP [98]. All reported concentrations are final concentrations.

2.2 Acquisition of fluorescent transients

In the ATP-induced actomyosin dissociation experiment, usually 0.5 μM actomyosin was rapidly mixed with ATP solution of variable concentrations. In the ADP inhibition of the ATP-induced actomyosin dissociation experiment, 0.5 μM actomyosin was rapidly mixed with the premixed ATP and ADP solution. The concentration of ATP in solution was 0.6 mM or 0.9 mM and the concentration of ADP varied from 20 to 200 μM. Transient fluorescence of pyrene-labeled actin was measured with a Bio-Logic SFM300 stopped flow transient fluorimeter (Bio-Logic Science Instruments SAS, Claix, France), equipped with an FC-15 cuvette (Figure 2.2). Usually, three syringes and two mixers were used in an experiment.

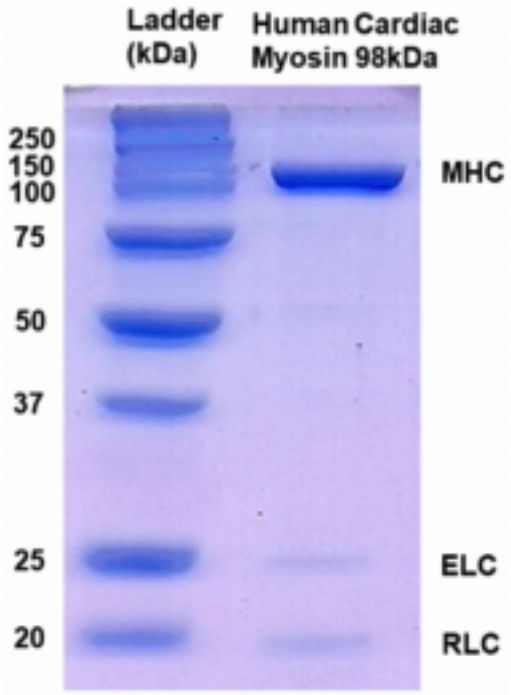

Figure 2.1: SDS-PAGE of the purified recombinant myosin head

*98 kDa human cardiac S1 co-purifes with murine ELC and RLC.

The continuous flow and the smallest inter mixer delay line (40 μL) were usually used. Myosin intrinsic fluorescence was excited by mercury-xenon lamp at 296 nm and detected using a 320 nm cutoff filter. The pyrene fluorescence was excited at 365 nm and detected using a 420 nm cutoff filter. Multiple transients were acquired and averaged to improve the signal to noise ratio. 8000 points were acquired in each experiment. For cardiac myosin, experiments were performed at T=20 °C, calcium and ficoll experiments were performed at T=12 °C . Transient experiments were performed with myosin constructs from at least three independent preparations.

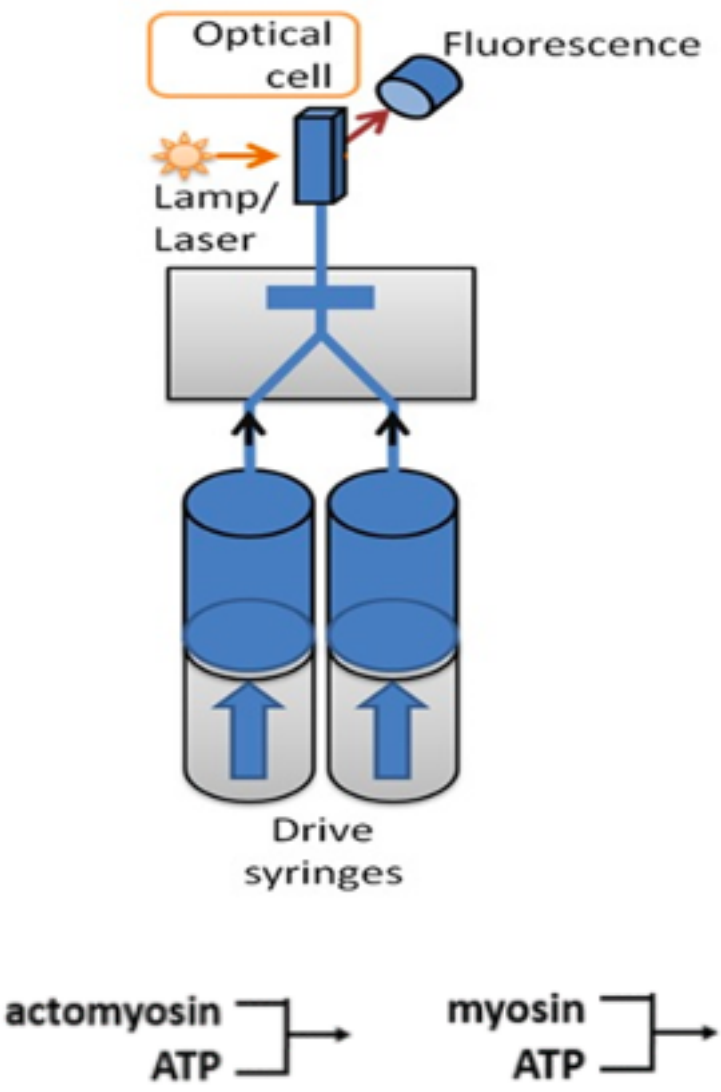

Figure 2.2: Schematics of the stopped flow apparatus

2.3 Analysis of fluorescence transients

The transients obtained in each experiment were fitted by the single exponential function $S(t)$=S_o + Aexp(− k_{obs}.(t − t_0)), or the double exponential function $S(t)$=S_o + A_1 exp(− k_{obs1} (t − t_0)) + A_2 exp(− k_{obs2} (t − t_0)). S(t) is the observed signal at the time t, A_i is the signal amplitude, t_0 is the time before the flow stops, and k_{obsi} is the observed rate constant. Transients, obtained for the same actomyosin preparation at different concentrations of the nucleotide were fitted together, assuming the known value of t_0, measured in a separate experiment, and the constant value of S_0, which depends on the concentration and labeling efficiency of pyrene-labeled actin in the actomyosin preparation. In the case of the double exponential global fit, we kept amplitudes of the transients constrained, $A_1 + A_2 = const$, to account for the conservation of mass. Transients of the ATP induced actomyosin dissociation were fitted with the single exponential function to determine the rate constant k_{obs}. The dependence of the observed rates on the ATP concentration was fitted by a hyperbola, $v = V_{max}[ATP]/(K_{app} + [ATP])$, allowing the determination of the maximum rate, V_{max} (the horizontal asymptote). In the case of the ATP-induced actomyosin dissociation, the rate constant k_{+2T} is the V_{max} and the equilibrium constant of the collision complex formation K_{1T} is $1/K_{app}$. To determine the bi-molecular rate ($K_{1T}k_{+2T}$, Scheme in Figure 2.3), the dependence of the observed rates on the ATP concentration was fitted by a straight line at small concentrations of ATP. All data fits with an exponential function, hyperbola, and polynomial were performed with Origin 8 (OriginLab Corp, Northampton MA). The statistical significance of results was tested with ANOVA integrated into Origin 8 software. A significance level of $P<.05$ was used for all analyses. We also fitted the acquired transients to the time-dependent numerical solution of differential equations corresponding to scheme in Figure 2.3 and scheme in Figure 2.4. The equations are shown in the Appendix section. The numerical solution was obtained using the built-in symbol NDSolve in Wolfram Mathematica. The

solution was fitted to an acquired transient using the built-in symbol NMinimize by minimizing the residual sum of squares. The scripts are shown in the Appendix section. The goodness of the fit was assessed with the Pearson χ^2 test, χ^2 was 98%-99% in all fits. Representative fits of the experimental data are shown in the results section. The signal intensity of transients was expressed in the units of actin concentration based on the assumption that all actomyosin is dissociated at the end of the reaction. The assumption is supported by our experimental observation that all transients of the same protein preparation have the same final amplitude of pyrene fluorescence, indicating complete dissociation of actomyosin at the end of the reaction. Transients obtained for the same actomyosin preparation were fitted globally. Data of at least three biological replicates were fitted, the obtained rate constants were averaged, and mean values and standard deviations are reported.

$$A{\cdot}M + T \underset{k_{-1T}}{\overset{k_{+1T}}{\rightleftarrows}} A{\cdot}M{\cdot}T \underset{k_{-2T}}{\overset{k_{+2T}}{\rightleftarrows}} A^* + M{\cdot}T$$

Figure 2.3: ATP-induced actomyosin dissociation

A = pyrene-labeled actin, M = myosin, T = ATP, A* = actin with unquenched pyrene fluorescence

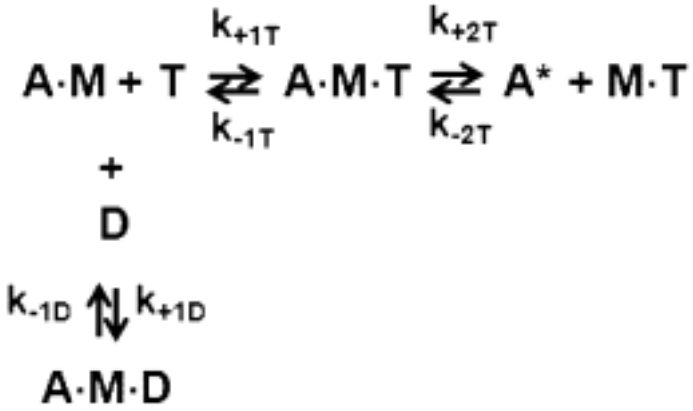

Figure 2.4: ATP-induced actomyosin dissociation, competitive inhibition with ADP

2.4 ATPase assays

Steady state basal and actin activated myosin ATPase activities were measured spectrophotometrically at T=12 °C in the buffer contained 20 mM MOPS pH 7.3, 50 mM KCl, and 5 mM $MgCl_2$ or $CaCl_2$, by mixing myosin or actomyosin with 5 mM MgATP or CaATP, with 10% or no ficoll, and monitoring the liberation of inorganic phosphate, as described previously [99]. Both myosin and F-actin were carefully washed before each experiment to avoid any possibility of contamination by products of hydrolysis, phosphate and ADP. Myosin or actomyosin was mixed with ATP, and aliquots were collected at equal time intervals and analyzed for phosphate in ammonium molybdate malachite green colorimetric assay. The rate of basal myosin ATPase V_{basal} was determined as the rate of phosphate production. To determine maximum velocity of the actomyosin ATPase, the rates of myosin ATPase at different actin concentrations were fitted by the hyperbolic equation $v = V_{basal} + V_{act}[actin]/(K_{app} + [actin])$, where v is the rate of the ATPase in the presence of actin, horizontal asymptote, $V_{max} = V_{basal} + V_{act}$, is the rate of myosin ATPase at infinite actin concentration. Normalized values for phosphate concentration at different reaction times (basal ATPase) and reaction rates at different actin concentrations (actin activated ATPase) obtained from experiments using several inde-

pendent preparations of actin and myosin were averaged and mean values and standard deviations were plotted and fitted with the line (basal ATPase) or with the hyperbola (actin activated ATPase) using Origin 8 (OriginLab Corp., Northampton MA). Determined ATPase rates (the value and the standard error) are presented in results section . We did not account for F-actin ATPase activity since this is a slow process [100], significantly inhibited by phalloidin [101].

2.5 Analysis of fluorescence transients- competitive inhibition reaction

Competitive inhibition of ATP-induced actomyosin dissociation by ADP was measured with pyrene labeled actin complexed with myosin and incubated with ADP at various concentrations, including [ADP]=0 μM. This solution was rapidly mixed with ATP, and the transient fluorescence of pyrene-actin dissociated from myosin was measured. The observed reaction rates were fitted globally to the equation $k_{obs} = V_{max}[ATP]/(K_d(1 + [ADP]/K_5') + [ATP])$ [102, 103, 61], with several common parameters: rate constant V_{max} (k_{+2}'), the equilibrium constant of actomyosin.ATP collision complex dissociation $K_d(1/K_1')$, and K_5', the equilibrium constant of ADP dissociation from actomyosin upon chasing with ATP (Figure 2.5).

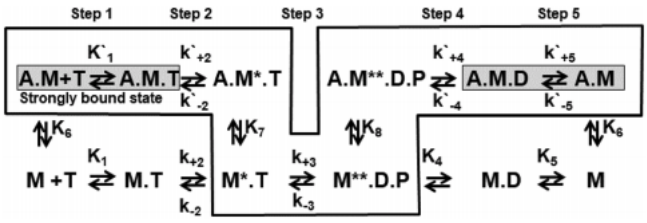

Figure 2.5: Actomyosin ATPase cycle reaction scheme

A actin, M myosin (M* and M** myosin states with increased intrinsic fluorescence, fluorescence in M** state is higher), T ATP, D ADP, P phosphate. Asterisk indicates reaction rate constants describing actomyosin kinetics. Highlighted strongly bound actomyosin state. Boxed generally accepted pathway of actomyosin interaction.

CHAPTER 3: RESULTS

3.1 Dead time of the transient spectrophotometer

Transients are fitted with single exponential function. Intercept of fitted lines corresponds to the time of the flow stop. Vertical dashed line shows the dead time of the spectrophotometer, 2.6 ms (Figure 3.2). This calibration gives us information on the parameter t_0 in the fitting equation $S(t) = S_o + Aexp(-k_{obs}(t - t_0))$, and the time point in the reaction kinetics, we should start the fit (12.6 ms in this case).

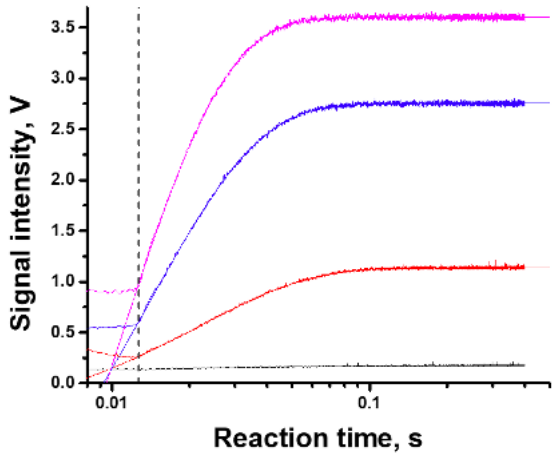

Figure 3.1: Dead time of the transient spectrophotometer

* 100 μM of 8-hydroxyquinoline mixed with 5mM (Purple trace), 2.5mM (Violet trace), 1mM (Red trace), and 0mM (Black trace)$MgCl_2$ [104].

* All concentrations are final.

* Flow rate is 8 mL/s per syringe.

3.2 ATP-induced actomyosin dissociation

ATP binds actomyosin in a two-step process (Figure 2.3). The first step is the rapid equilibrium when strongly bound actomyosin forms a collision complex with ATP, and $k_{1T} > k_{+2T}$. Pyrene fluorescence does not change during this step. Upon isomerization of the actomyosin-ATP collision complex, ATP binding results in irreversible dissociation of actomyosin. In our experiments, the formation of the actomyosin complex (prepared by mixing of expressed cardiac myosin constructs with the pyrene-labeled rabbit skeletal actin) led to decreased pyrene fluorescence. This decrease was similar for all myosin constructs, indicating strong binding of actin and expressed myosin constructs. When prepared actomyosin is rapidly mixed with ATP, the time course of pyrene fluorescence follows single exponential kinetics. The final amplitudes of all transients, obtained for the same preparation of actomyosin, were the same for all used concentrations of ATP, showing complete dissociation of actomyosin complex and confirming that the ATP-induced dissociation is irreversible.

Figure 3.2 shows a fluorescence transient observed for the WT myosin at 20 °C when 0.5 μM actomyosin is mixed with 900 μM ATP in the stopped-flow fluorimeter (all reported concentrations are in the final mixture, here and throughout the text). The observed rate constants for the WT myosin and the mutants depend on ATP concentration hyperbolically (Figure 3.3), the reaction rate constant k_{+2T} and the association constant of the collision complex K_{1T} can be determined from the fit to a hyperbola. The second-order association rate constant ($K_{1T}k_{+2T}$) is determined at small concentrations of ATP (Figure 3.4) when the dependence of the reaction rate on ATP is linear [102]. We determined all kinetic constants, shown in 2.3 in the fit of obtained transients to the numerical solution of differential equations (Appendix A) (Table 3.1).

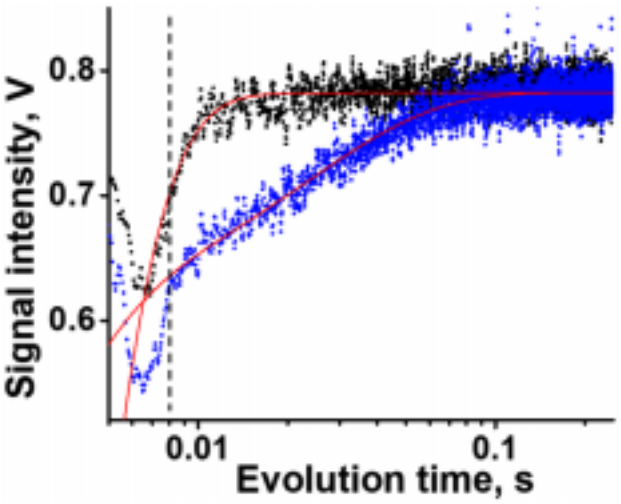

Figure 3.2: ATP-induced actomyosin dissociation with and without ADP

* Actomyosin (0.5 μM) rapidly mixed with ATP (upper trace, black), or the mixture of ATP and ADP (lower trace, blue).

* [ATP] = 900 μM in both cases [ADP] = 200 μM when present in the mixture.

* Final pyrene fluorescence is the same, indicating complete actomyosin dissociation regardless of the concentration of ADP used.

* Fitting curves (red) are single exponential function (upper trace, the actomyosin + ATP experiment) and double exponential function (lower trace, the actomyosin + (ATP + ADP) experiment).

* Dead time, measured in a separate experiment, constrains the fit (all fits intercept at the mixing time in the bottom left corner).

* The vertical dashed line shows the time of the flow stop and the beginning of the fit.

* Meaningful kinetic traces lay on the right side of the dashed line. On the left, there are flow artifacts.

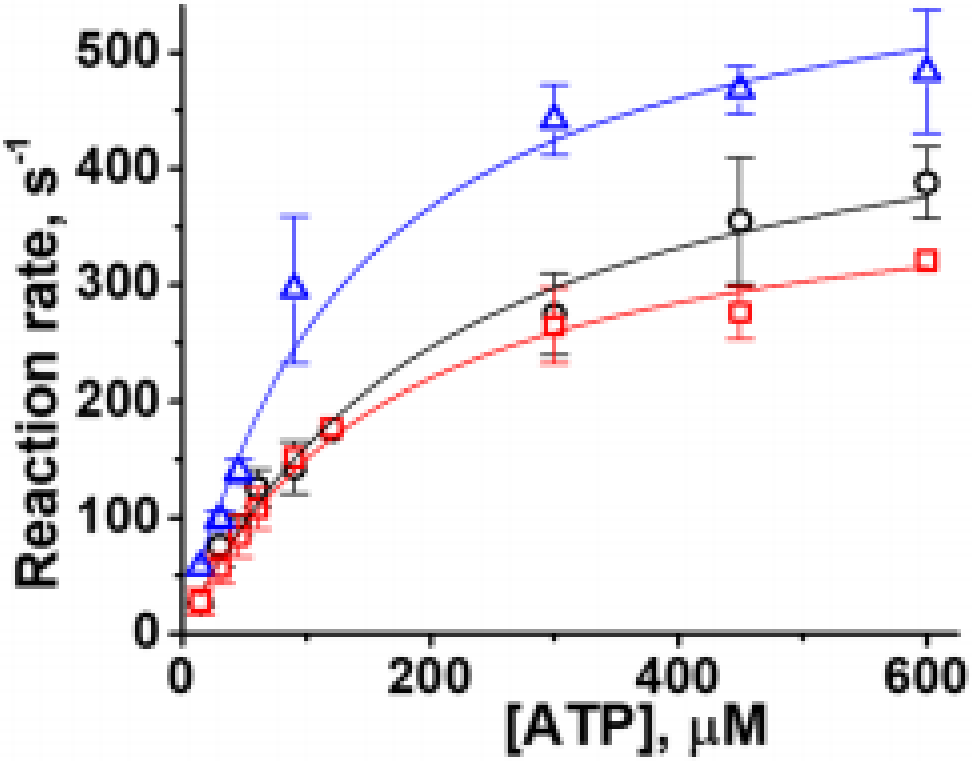

Figure 3.3: Rate of ATP induced actomyosin dissociation

* Black circles, WT, N = 3, red squares, R694N mutant, data from [62].

* N = 3 (the point at [ATP] = 600 μM, N = 1), blue triangles, E45Q mutant.

* Reaction rates fitted with a hyperbola.

* $k_{+2T} = 491.5 \pm 74.1 s^{-1}$ for WT mutant.

* $k_{+2T} = 338.8 \pm 47.8 s^{-1}$ for R694N mutant.

* $k_{+2T} = 618.5 \pm 75.3 s^{-1}$ for E45Q mutant.

* Data points are $mean \pm SD$. N is the number of biological replicates.

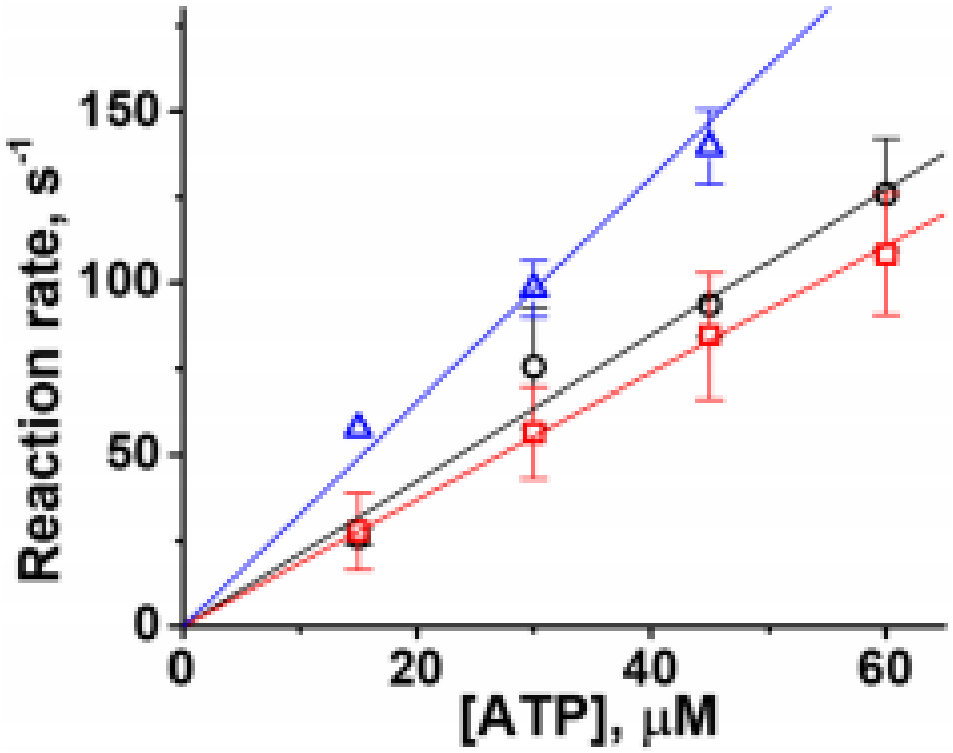

Figure 3.4: Second-order reaction rate of ATP induced actomyosin dissociation

* Observed reaction rates at low [ATP] are fitted by a straight line, the second-order reaction rate constant is determined from the slope of the line.

* Black circles, WT, N = 3, $K_{1T}k_{+2T} = 2.12 \pm 0.21\ \mu M^{-1}s^{-1}$.

* Red squares R694N mutant, N = 3, $K_{1T}k_{+2T} = 1.85 \pm 0.03\ \mu M^{-1}s^{-1}$

* Blue triangles, E45Q mutant, N = 3, $K_{1T}k_{+2T} = 3.27 \pm 0.31\ \mu M^{-1}s^{-1}$

* Data points are $mean \pm SD$. N is the number of biological replicates. Data from [62].

We calculated constants K_{1T} and $K_{1T}k_{+2T}$ to compare with the constants obtained in the fit of the transients to a single-exponential function, and the following fit to a hyperbola and a straight line. We found a good agreement of the kinetic constants, obtained by two fitting methods. Obtained in the fit to a hyperbola and in the fit to the numerical solution of differential equations (Appendix A). There is no significant differences observed for the equilibrium constant K_{1T} between the WT and mutants. The second-order association rate constant $K_{1T}k_{+2T}$ of E45Q mutant show a 1.5 times higher rate compared to WT Table 1.1 .

3.3 ADP dissociation from actomyosin

ADP has a high affinity to the WT human cardiac actomyosin. The equilibrium dissociation constant of ADP is in the micromolar range [61, 62]. To measure the rate of ADP dissociation from actomyosin we rapidly mix pyrene-labeled actomyosin with premixed ADP and ATP. In our experiments, we kept ATP concentration constant (near saturation, but not saturated, 600 μM or 900 μM) and vary ADP concentration from 20 to 200 μM. Upon mixing, actomyosin can bind either ATP or ADP and form either an actomyosin-ATP or actomyosin-ADP complex (Figure 2.4). ATP binding results in actomyosin dissociation and increased pyrene fluorescence. ADP binding does not dissociate actomyosin and therefore does not change the intensity of pyrene fluorescence. If actomyosin, actomyosin-ATP, and actomyosin-ADP complexes are in rapid equilibrium, compared to the rate of ATP induced actomyosin dissociation, we should observe a single-exponential increase of pyrene fluorescence, corresponding to the competitive inhibition of the ATP-induced actomyosin dissociation. At the saturated concentration of ATP, there should be no ADP dependence on the rate of actomyosin dissociation [102]. In our experiments with the constructs of human cardiac myosin, we usually observe the double-exponential kinetics of ATP-induced actomyosin dissociation in the presence of ADP (Figure 3.2). Our observation of the double-exponential kinetics suggests that

there is no rapid equilibrium in the mixture of actomyosin, ATP, and ADP on a timescale of actomyosin dissociation. ADP readily binds actomyosin, and the rate of ADP dissociation from actomyosin is slower or comparable with the rate of ATP-induced actomyosin dissociation. The range of ADP concentrations in this experiment was suggested by the resolution of kinetic components of a transient. At small concentrations of ADP ([ADP] $< 20\ \mu$M) we observed a single-exponential transient with the rate constant corresponding to the rate of ATP-induced actomyosin dissociation. This observation shows that the probability of ATP binding is higher due to a significantly higher concentration of ATP. At large concentrations of ADP ([ADP] $> 200\ \mu$M) we observed a single-exponential transient with the rate, slower than the rate of ATP-induced actomyosin dissociation. This observation shows that at high concentration ADP preferentially binds actomyosin instead of ATP, and the rate of ATP-induced actomyosin dissociation is modulated by the rate of ADP binding, and, most likely, by several consecutive ADP bindings. The rate of the fast component of the observed double-exponential kinetics does not depend on ADP concentration. We conclude that there is no fast exchange between ADP and actomyosin.ADP complex in the beta isoform actomyosin, wild type, and mutants. The rate of the slow component of double-exponential transient depends on the concentration of ADP and reflects ADP binding to actomyosin, followed by ADP dissociation and subsequent ATP binding, resulting in actomyosin dissociation. To determine the rate of ADP binding to and ADP dissociation from actomyosin we fit the acquired transients globally to the numerical solution of differential equations (Appendix A), corresponding to Figure 2.4. In the fit, we used the rate constants, previously determined for the ATP-induced actomyosin dissociation reaction, and varied only the rates k_{+1D} and k_{-1D}. The fit shows that ADP dissociates faster from actomyosin with mutant R694N and E45Q mutants compared to WT.

Table 3.1: Kinetic rate constants for HC myosin

	WT	R694N	E45Q	D208Q:K450L	I303V:I313V
Actomyosin Dissociation					
$k_{+2T}(s^{-1})$	406.2 ± 14.1	449.1 ± 55.5	619 ± 52.3	428.67 ± 24.97	1010.87 ± 30.81
$K_{1T}k_{2T}(\mu M^{-1}s^{-1})$	4.6 ± 1.0	3.0 ± 0.9	7.6 ± 1.9	3.26 ± 0.08	3.41 ± 0.02
Actomyosin Collision Complex Formation					
$K_{1T}(mM^{-1})$	11.2 ± 2.4	6.8 ± 1.8	12.3 ± 2.8	10.63 ± 1.52	4.1 ± 0.24
ADP Binding to and Release from Actomyosin					
$k_{+1D}(\mu M^{-1}s^{-1})$	26.6 ± 8.1	94.7 ± 52.1	82.6 ± 4.3	11.53 ± 4.98	9.58 ± 2.15
$k_{-1D}(s^{-1})$	199.6 ± 51.8	776.1 ± 285.3	301.3 ± 74.3	60.62 ± 6.79	83.12 ± 4.57
ADP Dissociation from Actomyosin					
$K_{1D}(\mu M)$	7.5 ± 3.0	8.2 ± 5.4	3.6 ± 0.9	6.14 ± 2.08	9.0 ± 1.57

3.4 Rates of basal and actin-activated myosin CaATPase activity

Actin activation is defined as the increased rate of myosin ATPase activity in the presence of actin. Our data show about 20-fold increase of actin activation of myosin MgATPase activity (Figure 3.6). the rate of basal CaATPase is 50 times higher than the rate of MgATPase (Figure 3.5). The value of actin activation (V_{max}/V_{basal}) of myosin CaATPase is just two-fold, smaller than the value for MgATPase (20-fold).

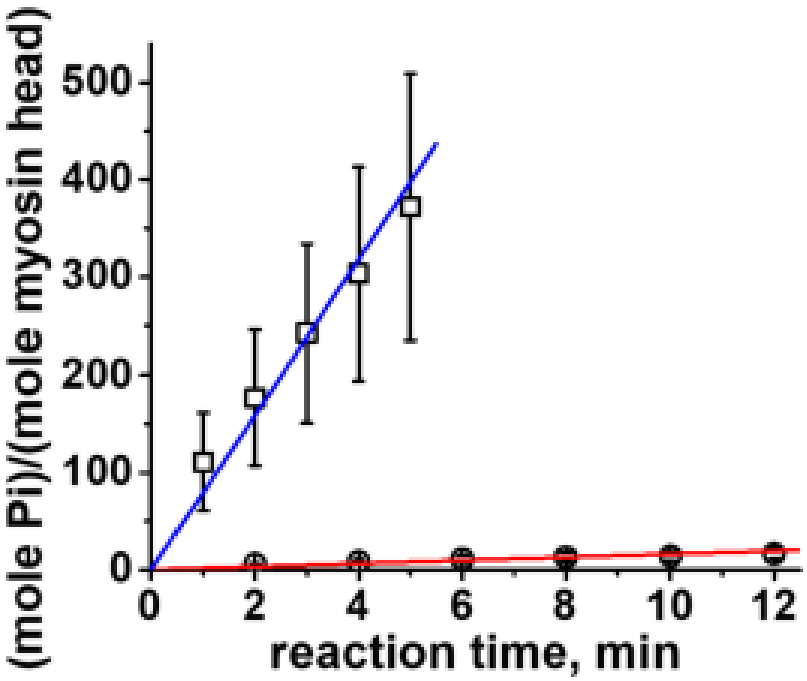

Figure 3.5: Steady state basal ATPase activity

* Basal myosin ATPase activity, [myosin] = 3.3 μM, [ATP] = 5 mM.

* Circles, MgATP, squares, CaATP. Linear fit.

* The data points are averages of N = 3 (Mg) and N = 4 (Ca) independent protein preparations.

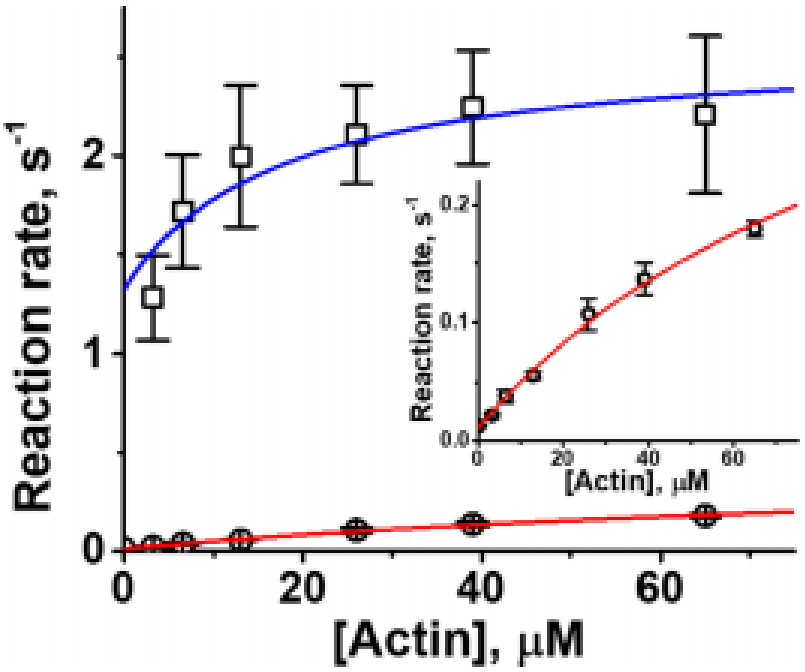

Figure 3.6: Steady state actin-activated ATPase activity

* Steady state actin activated myosin ATPase activity, [myosin] = 0.8 μM, [ATP] = 5 mM.

* Circles, MgATP, squares, CaATP. Line, fit with a hyperbola, $V_{basal} + V_{max}[actin]/(K_{app} + [actin])$.

* Inset, MgATPase. The data points are averages of N = 3 (Mg) and N = 2 (Ca) independent protein preparations

3.5 CaATP promotes futile recovery stroke

The rate of ATP-induced myosin conformational change was measured using 0.5 μM myosin S1 (here and throughout the text the concentration in the final mixture is given), rapidly mixed with various concentrations of MeATP, where Me = Mg or Ca. Myosin intrinsic fluorescence changes upon mixing with ATP. Observed transients were fitted with one (Mg) or two (Ca) exponentials (Figure 3.7). Both metal cations sustain myosin ATPase activity, showing the increase of M** population (myosin high fluorescence state)

upon mixing myosin S1 with ATP. Maximum rate of myosin conformational change V_{max} is the same within experimental error for both cations (Figure 3.8). Our data also show that in the presence of CaATP, myosin reaches the M** state. However, the M** state depopulates with the rate $0.99 \pm 0.08\ s^{-1}$, and the equilibrium is established at the lower level of myosin intrinsic fluorescence.

This behavior indicates that the equilibrium between the M** and M* states is shifted towards the M* state in the presence of CaATP. The rate of depopulation of the M** state does not depend on CaATP concentration. Therefore, the lifetime of the M** state in myosin CaATPase is a constant value, which is shorter than the lifetime of the M** state in myosin MgATPase. The rate of the M** state depopulation in myosin CaATPase corresponds well to $1/V_{max}$ of the basal myosin CaATPase. We interpret observed depopulation of M** state in the presence of calcium as faster Pi release, followed by ADP release. Slow ADP release should result in deeper drop of myosin intrinsic fluorescence in (Figure 3.7), not observed in our experiments. We exclude weak CaATP binding to myosin in interpretation of observed transient kinetics, since CaATP binds tighter to myosin than MgATP ($K_{appMg} > K_{appCa}$, Table 3.2), and observed depopulation of M** state does not depend on ATP concentration. Myosin lifetime in the M** state in the presence of calcium is long enough for myosin head to bind the thin filament.

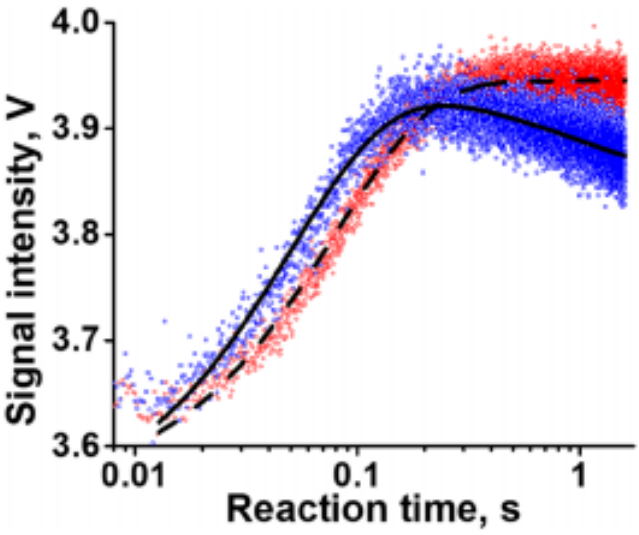

Figure 3.7: Ca ATP promotes futile myosin stroke

* Myosin intrinsic fluorescence transients upon rapid mixing of myosin and ATP.

Myosin 0.5 μM, MeATP 10 μM.

* Me =Mg, red dots, experiment, and dashed line, single exponential fit.

* Me = Ca, blue dots, experiment, and solid line, double exponential fit.

* The second exponent in the case of CaATP does not depend on [CaATP], the rate is

$0.99 \pm 0.08\ s^{-1}$

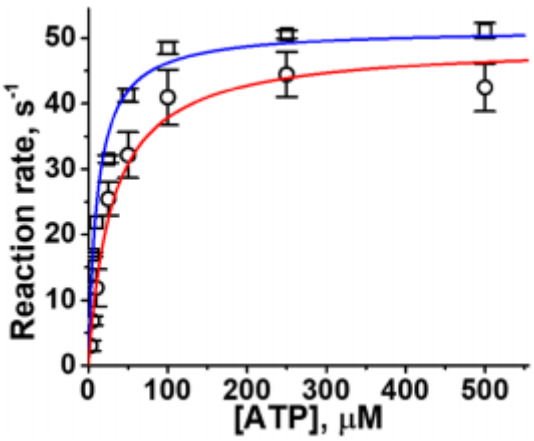

Figure 3.8: Rate of recovery stroke

* Kinetics of ATP binding and recovery stroke upon rapid mixing of myosin and ATP.

* Observed rate constants are fitted with a hyperbola.

* $V_{max} = 49.0 \pm 2.4\ s^{-1}$ for MgATP (circles, N = 3)

* $V_{max} = 51.4 \pm 2.3\ s^{-1}$ for CaATP (squares, N = 2)

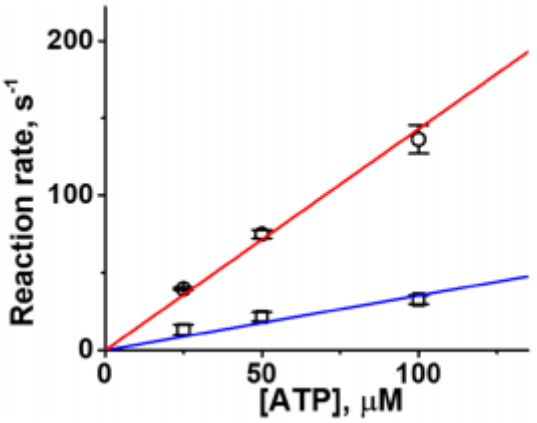

Figure 3.9: Second-order reaction rate of ATP induced actomyosin dissociation

ATP-induced actomyosin dissociation. Observed reaction rates at low [ATP] are fitted by a straight line, the second order reaction rate constant is determined from the slope of the line.

3.6 Effect of ficoll micro-environment on myosin kinetics

We have used the wild-type rabbit skeletal myosin S1. Addition of 10% w/v ficoll led to the faster rate of ATP induced actomyosin dissociation. The kinetics of ADP dissociation from actomyosin is best fitted to the two-exponential function. One component of the kinetics transient reflects ADP dissociation,which was slower than the rate of ADP dissociation without ficoll in solution. Our data show that ADP binds actomyosin stronger in the presence of ficoll. The rate of the second component of the transient does not depend on the concentration of nucleotide in solution (Table 3.3).

Table 3.2: Kinetic rate constants for Mg and Ca ATP

	Mg	Ca
Basal myosin ATPase, (mole Pi. (mole myosin head)$^{-1}.s^{-1}$)	0.03 ± 0.002 (N=3)	1.33 ± 0.07 (N=4)
Actin-activated myosin ATPase, V_{max}, (mole Pi. (mole myosin head)$^{-1}.s^{-1}$)	0.5 ± 0.11 (N=3)	2.58 ± 0.33 (N=2)
Actin-activated myosin ATPase, K_{app}, (μM)	111.5 ± 37.3 (N=3)	17.2 ± 11.6 (N=2)
ATP binding to myosin, dissociation constant K_d, (μM)	29.8 ± 3.1(N=3)	2.67 ± 0.57(N=2)
Recovery Stroke and hydrolysis, $k_{+3} + k_{-3}$, (s^{-1})	49.0 ± 2.4 (N=3)	51.4 ± 2.3 (N=2)
ATP induced actomyosin dissociation, K'$_1 k'_{+2}$, (μM$^{-1}s^{-1}$)	1.43 ± 0.06 (N=3)	0.35 ± 0.04 (N=3)
ATP induced actomyosin dissociation, k'$_{+2}$, (s^{-1})	543.9 ± 22.7 (N=3)	173.6 ± 13.9 (N=3)
Actomyosin.ATP collision complex formation, K_d, (μM)	263.6 ± 25.4(N=3)	530.5 ± 80.0(N=3)
ADP release from actomyosin, K'$_5$, (μM)	179.4 ± 17.5(N=3)	293.2 ± 38.2(N=3)

The data averages of N independent protein preparations

Table 3.3: Kinetic rate constants for Rabbit skeletal myosin in the presence of Ficoll

	No Ficoll	with Ficoll
Basal myosin ATPase, (mole Pi. (mole myosin head)$^{-1}$.s^{-1})	0.0022 ± 0.0009 (N=6)	0.0019 ± 0.0007 (N=3)
ATP binding to myosin, dissociation constant K_d, (μM)	263.6 ± 25.4 (N=3)	588.9 ± 79.6 (N=3)
ATP induced actomyosin dissociation, K'$_1 k'_{+2}$, (μM$^{-1}s^{-1}$)	1.43 ± 0.08 (N=3)	1.74 ± 0.08 (N=3)
ATP induced actomyosin dissociation, k'$_{+2}$, (s^{-1})	543.9 ± 22.7 (N=3)	1107.5 ± 88.3 (N=3)
Actomyosin.ATP collision complex formation, K_d, (μM)	263.6 ± 25.4 (N=3)	199.2 ± 23.9 (N=3)
ADP release from actomyosin, K'$_5$, (μM)	179.4 ± 17.5 (N=3)	103.6 ± 14.6 (N=3)

The data averages of N independent protein preparations

CHAPTER 4: Discussion

The work presented in this thesis has focused on gaining a deeper understanding of the dynamics between electrostatic interactions within the myosin head domain and its kinetic performance *in vitro*. I have described the development of four novels, human cardiac myosin (β-isoform) mutant constructs: R694N, E45Q, D208Q: K450L, and I303V: I313V. These mutant constructs reconstitute the head domain (S1) of HC myosin β-isoform with mutations induced by site-directed mutagenesis. These constructs were leveraged to characterize the kinetic performance of HC myosin β-isoform *in vitro*. In the next sections, I will discuss the implications of these findings for our understanding of the regulation of HC myosin β-isoform.

4.1 Models for characterizing ADP dissociation from actomyosin

The results obtained with the competitive binding of ATP in the presence of ADP assay described in this thesis highlight several key parameters namely, equilibrium dissociation constant of ADP, ADP binding, and release from actomyosin. Data obtained from this reaction can be analyzed using multiple schemes that explain the strong binding of ADP to actomyosin observed in our experiments. As described in the methods section, by mixing pyrene-labeled actomyosin with premixed ADP and ATP, the rate of ADP dissociation can be quantified.

Conventional models describe this reaction as a classic enzyme kinetics competitive inhibition scheme (Figure 4.1). Increased intensity in pyrene-fluorescence is observed when ATP binds to actomyosin and dissociates actin from myosin. The rate constants for this reaction are described by the rate constants k_{+1T} and k_{+2T}. A parallel reaction, ADP binding to actomyosin does not dissociate actomyosin, forms actomyosin.ADP

complex (Figure 4.1). ATP-induced actomyosin dissociation in the presence of ADP is correlated to the equilibrium rates of the two parallel reactions.

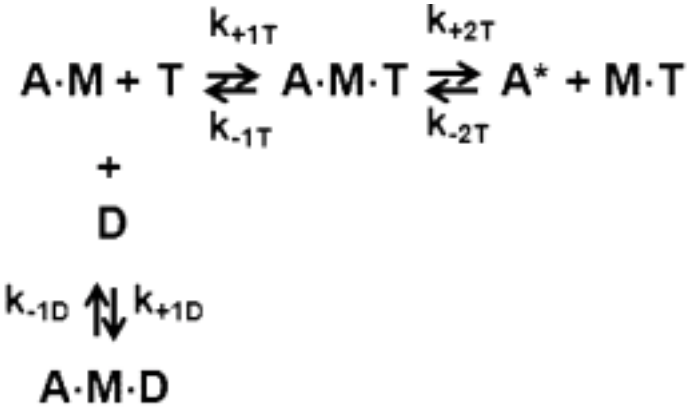

Figure 4.1: ATP induced actomyosin dissociation, competitive inhibition with ADP

The competitive inhibition model predicts a rapid equilibrium between actomyosin.ATP and actomyosin.ADP complexes, relative to the rate of ATP-induced actomyosin dissociation [102]. Additionally, the competitive inhibition model, predicts a single exponential fluorescence trace ATP-induced actomyosin dissociation in the presence of ADP. In our experiments with human cardiac myosin constructs, we observe a double exponential fluorescent trace corresponding to this reaction (see results section). The double exponential has two components, fast and slow. The fast component corresponds to the ATP-induced actomyosin dissociation, whereas the slow component corresponds to ADP binding to actomyosin, and thereafter delayed ATP-induced actomyosin dissociation.

While the competitive inhibition model is well-suited to explore the impact of ADP on ATP-induced actomyosin dissociation, does not accurately explain the fast and slow components of actomyosin.ATP and actomyosin.ADP interactions respectively. An outstanding question is the role of ADP dependence on the fast component of actomyosin dissociation. Our results indicate an absence of rapid equilibrium between actomyosin and actomyosin.ADP complex. To our knowledge, this is the first demonstration that human cardiac myosin follows double-exponential kinetics in the presence of ATP and

ADP.

Several factors could account for the differing results observed. It would be interesting to explain the observed kinetic behavior with an alternative model. Based on the similarity in size and structure of ADP and ATP, we propose a two-step sequential model for ATP-induced actomyosin dissociation, inhibited by ADP (Figure 4.2). The proposed model follows parallel reactions similar to the competitive inhibition model (Figure 4.1). In the first path, actomyosin interacts with ATP in two sequential steps and induces actomyosin dissociation. These steps are characterized by rate constants k_{+1T} and k_{+2T}.In the second path, actomyosin interacts with ADP in two sequential steps similar to actomyosin.ATP interaction (Figure 4.2). Prior work has proposed a two-step sequential actomyosin.ADP interactions in the ATPase cycle [103, 105, 43, 50, 106].

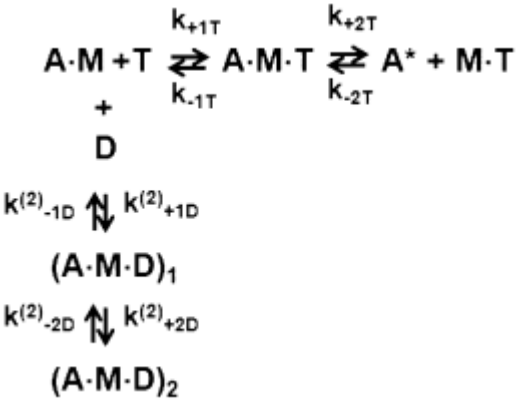

Figure 4.2: Two-step sequential model for ATP induced actomyosin dissociation, competitive inhibition with ADP

Although our data do not support this model, it may enable more extensive, characterization of mutant constructs, change population states between consecutive states of actomyosin.ADP, proposed in the two-step sequential model (Figure 4.2). Two mechanisms to explain the actomyosin.ADP interaction could be envisioned. First, the competitive inhibition model (Figure 4.1), characterizes diffusion-controlled actomyosin.ADP interaction step by kinetic parameters k_{-1D} and k_{+1D}. Absence of rapid equilibrium between

actomyosin, actomyosin.ATP, and actomyosin.ADP dictates $k_{-1D} \leq$k$_{-+2T}$. Second, the two-step sequential model characterizes two actomyosin.ADP states: $(A.M.D)_1$ and $(A.M.D)_2$ (Figure 4.2). To satisfy the condition of rapid equilibrium observed in the data obtained, the rate $k^{(2)}_{-1D}$ should be larger than $k^{(1)}_{-1D}$ but smaller than $k^{(1)}_{+1T}$. A subset of myosin heads populated in $(A.M.D)_1$ and $(A.M.D)_2$ states, can be determined by the dissociation constants $1/K^{(2)}_{2D}$ and $1/K^{(2)}_{1D}$ respectively [107]. It remains to be determined whether the overall charge of the nucleotide-binding site on myosin plays a role in the observed difference in rates of ATP and ADP binding to actomyosin.

4.2 Potential for regulating myosin by disrupting electrostatic interactions on the head domain

4.2.1 Timing of the strongly bound state

The mutants R694N and E45Q show a faster rate of ADP dissociation from actomyosin , and therefore, shorter duration of the strongly bound actomyosin state, t_s. The timing of the strongly bound state depends on how fast actomyosin exits the state, $ts = 1/k_{+2T} + 1/k_{-1D}$, where k_{+2T} is the rate of ATP-induced actomyosin dissociation, and k_{-1D} is the rate of ADP dissociation from actomyosin. For the WT β- isoform human cardiac myosin $ts = 7.5 \pm 1.3$ ms, for the R694N mutant $ts = 3.5 \pm 0.5$ ms, 47% shorter. Mutation E45Q, disrupting the isoform-specific salt bridge R694:E45, which is responsible for the electrostatic interactions between SH2 helix and SH3-like domain of the myosin head, also leads to the shorter timing of the strongly bound state of actomyosin, $ts = 4.9 \pm 0.8$ ms. Structural details of such regulation of myosin kinetics are yet to be determined. If in the WT and the E45Q constructs the rate k_{-1D} of ADP dissociation from actomyosin is slower than the rate k_{+2T} of ATP-induced actomyosin dissociation, and therefore, the time of ADP release governs the time of the strongly bound state of actomyosin. In the R694N construct, the rate k_{1D} of ADP release from actomyosin statistically equal to the rate k_{+2T} of ATP-induced actomyosin dissociation, then the time of the strongly bound

state is determined by two of these processes.

4.2.2 Equilibrium States of cardiac myosin active state

The hyperbolic dependence of ATP-induced actomyosin dissociation indicates that ATP binds actomyosin in two steps, first forming the collision actomyosin-ATP complex, which is in rapid equilibrium with ATP and actomyosin, and then binding actomyosin practically irreversibly, causing actomyosin dissociation. All mutants and the WT myosin construct exhibit that hyperbolic dependence. Our fits show that the rate of the collision complex formation k_{+1T} is slower than the rate of the diffusion-controlled bi-molecular reaction for both mutants and the WT actomyosin. This can be interpreted as if the active site is not open all the time and is in equilibrium between the open and closed states. It is interesting to mention that our fits give the rate of the collision complex dissociation k_{1T} of the same order of magnitude that the rate of the ATP-induced actomyosin dissociation k_{+2T}. Knowing the rate of the collision complex dissociation, one can determine the half-lifetime of the collision complex as $t_{1/2} = ln(2)/k_{-1T}$.

4.2.3 Charge dependent kinetics of cardiac myosin

Our fits for R694N and E45Q mutants, show that ADP binds actomyosin faster than ATP, possibly reflecting the difference in charge of these molecules. At pH 7 and higher, both MgADP and MgATP are ionized [108], and the total charge of MgADP and MgATP is $(-1e)$, and $(-2e)$ accordingly. This charge dependence of the kinetics of nucleotide binding may indicate an overall negative charge of the myosin active site, and therefore electrostatic repulsion when nucleotide binds actomyosin.

4.3 Myosin micro-environment and its regulation

In a functional muscle, the contractile unit sarcomere hosts myosin motors, that convert chemical energy to mechanical work. The micro-environment of myosin plays an instrumental role in shaping force generation. Our present study using the rabbit skele-

tal myosin model reveals that calcium ion concentration and macromolecular crowding regulates the individual steps in the myosin ATPase cycle. Work from our laboratory has deepened the understanding of the myosin regulation process by extending these findings from rabbit skeletal myosin models to other myosins including cardiac myosin.

Previous PFG NMR results show that the rate of ATP binding to actomyosin is similar to a diffusion-controlled reaction [109]. Additionally, studies on myosin.Ca.ADP and myosin.Mg.ADP binding to actin show similar rates [110]. In this thesis, we demonstrate that basal ATPase and actin-activated ATPase rates for CaATP are higher compared to Mg.ATP (see results section). It should be noted that the first-order binding rate of CaATP is higher relative to MgATP. A tighter binding of CaATP to myosin is also observed compared to the MgATP binding to myosin. Taking these factors into account, we can predict that under physiological conditions, in sarcoplasm, where Magnesium concentration is much higher than calcium concentration, the majority of myosin heads (up to 90 %) bind to Mg.ATP and orchestrate muscle contraction. But during MH, with elevated calcium levels, a fraction of myosin heads (up to 34 %), bind to CaATP [111].

Under physiological conditions, intracellular calcium levels are relatively low compared to magnesium concentration. ATP binds Ca^{+2} and Mg^{+2} with similar affinity. During malignant hypothermia (MH) conditions, cellular homeostasis is disrupted, leading to elevated intracellular, more specifically, myoplasm calcium levels. Three times higher intracellular calcium levels are observed in patients suffering from MH [88]. Several factors contribute to the observed elevated levels of myoplasm calcium concentration in MH patients. The elevated temperatures during MH, relative to normal physiological temperature, may alter the permeability of the sarcoplasmic reticulum (SR) [112]. Thermogenesis is hypothesized to be a consequence of upregulated MgATP consumption by myosin heads in the muscle cells, which is in turn caused by troponin upregulation, and by SERCA pumping excess calcium into the SR. The experiments described in this thesis (Methods section) establish a molecular mechanism for muscle rigidity observed

during MH.

Our observation described in this thesis, suggests that myosin and actomyosin kinetics in the presence of calcium show that myosin undergoes a futile recovery stroke with CaATP (see results section). It should be noted that basal myosin CaATPase activity is 50 times faster than MgATPase. Consistent with the prediction that during MH, increase sarcoplasm calcium levels, lead to elevated temperatures (thermogenesis); we hypothesize that futile myosin recovery stroke in the presence of Ca.ATP might be one of the reasons for excessive ATP consumption, which ultimately leads to the observed thermogenesis.

We have used macromolecular crowding agent Ficoll PM 70 to mimic the intracellular environment and study the effect of crowding on the kinetics of actomyosin dissociation and ADP release. Our previous studies of the heavily mutated *D. discoideum* myosin S1 construct showed that the effect of macromolecular crowding results in a more compact state of the myosin head. In agreement with the excluded volume theory, ficoll increased the rate of ATP induced actomyosin dissociation. Observed results can be interpreted as the kinetics of myosin conformational change, leading to the opening of the active site for nucleotide to bind. We infer that macromolecular crowding not only increases the chemical potential of solutes, but affects protein structural state due to change in the osmotic pressure.

4.4 Random mutagenesis of myosin constructs offer unique insights into human cardiac myosin isoforms differences

The electrostatic interaction disruption-based myosin regulation described in this thesis enabled elucidation of protein engineering mechanisms to understand the biochemistry of cardiac myosin function. Exploration of inter-residue electrostatic interactions gave rise to knowledge on the structural transition states of the cardiac myosin ATPase cycle. Inter-residue interactions vary dramatically in origin and their impact on regu-

lating cardiac myosin function. Electrostatics and dispersion are physical forces on an inter-atomic scale. Dispersion is a short-range force (r^{-6} range) and electrostatic force between charged residues is a long-range force (r^{-2} range).

Site-directed mutagenesis is a traditional molecular tool developed to engineer macromolecules including proteins and understand the role of submolecular elements within the proteins. The research field of myosin motor protein, relied on mutagenesis-based investigation methods for over five decades, to identify the functions of submolecular elements within a spectrum of myosin motor protein classes. In the introduction section, I described the rationale for the choice of proposed cardiac myosin mutant constructs. We demonstrated the importance of electrostatic interactions between charged residues of the structural elements within the myosin head domain, responsible for its *in vivo* and *in vitro* kinetics. Here, I will briefly discuss, a random mutagenesis strategy, that may assist in understanding the structural and functional differences between the two human cardiac myosin isoforms.

Sequence alignment studies of human cardiac myosin isoforms resulted in 80 differences between the two isoforms, out of which, 40 conserved differences were found in the motor domain[61]. These differences are distributed homogeneously across the motor domain. RLC and residues with direct nucleotide contact show no sequence changes [61]. Surface loops (see introduction section) well known for their variability contain differences and are known for their modulation of myosin motor properties [63, 113]. Loop 1 and Loop 2 modulate the interaction of myosin with actin and nucleotide respectively. Unfortunately, only available studies are on mouse cardiac muscle isoforms consisting of chimeras of Loop 1 and 2, which showed very few changes in the behavior of myosin [114]. This demands a search for other sites on the motor domain, which explain the behavior difference between the two isoforms.

A random mutagenesis study could be performed instead of a site-directed approach on β-isoform to fish out the hidden site differences between the two isoforms, which

contribute to their respective kinetic behavior. Some of these mutations may potentially convert its kinetic performance similar to α-isoform. Identifying the structural changes induced in the mutant isoforms that potentially mimic α-isoform kinetics helps us in understanding the structural differences between the two isoforms that contribute to their kinetic differences. Therefore, random mutagenesis serves as a tool (a) To fill the gap in the literature knowledge about the sites that contribute to the structural differences between two isoforms and (b) May create potential β-isoform mutants with accelerated kinetic performance.

The Discovery of a potential small molecule inhibitor that assists β-isoform mimic α-isoform kinetics may induce intramolecular conformational changes during the myosin ATPase cycle. Additional crystal studies on drugs along with β-isoform could deduce the induced structural changes within the molecule. Identification of the chemical structure of the drug and the motif of the protein it is interacting with will pave way for synthesizing the truncated small molecule that interacts with cardiac myosin and alter its kinetics *in vivo*.

4.5 The future of therapeutic development targeting myosin regulation

Although traditional drugs/therapeutics used for treating cardiovascular diseases like Heart failure and Cardiomyopathies, targeted the regulation of intracellular calcium levels, they resulted in severe side effects. Complete loss or weakened cardiac contractility is a hallmark in these pathological conditions. Clinical studies on these drugs demonstrated their ability to improve contractility. But this is achieved with some terrible consequences. Increased intracellular calcium ion concentration, enhances myocardial oxygen consumption, which triggers an elevated heart rate that ultimately leads to arrhythmia and ischemia.

Recent advances in our understanding of the molecular mechanisms of these illnesses have overturned the way therapeutics are designed. Small-molecule modulators of car-

diac myosin being developed to directly interact with cardiac myosin heads within the muscle cell sarcomere and thereby regulate its performance *in vivo*. These therapeutics are categorized under a class of drugs known as sarcomere-activating drugs. Mavacamten, Omecamtiv Mecarbil, and Levoismenden are few drugs that illustrate the efficacy of this novel strategy. Furthermore, clinical trial studies on these drugs reveal that they can directly activate cardiac myosin *in vivo* and enhance its performance [115, 116]. Unfortunately, further studies need to be carried out on the activation and inhibition of myosin activity *in vivo*.

Researchers in the field traditionally followed a top-down approach (high throughput assays) to isolate small-molecules therapeutics that can bind to myosin and regulate its kinetic performance and force-generating capability. A theme that emerges from this thesis is that further clinical development can be driven by novel biochemical insights made on the electrostatic network of myosin head domain, a bottom-up approach. To this end, we have developed and characterized novel cardiac myosin mutant constructs engineered to alter its normal behavior.

Although many facets of the electrostatic network in the myosin motor domain remain to be explored, our in vitro studies reinforce that the biochemistry of the myosin microenvironment dictates its activity that could be radically different *in vivo* compared to dilute solution studies performed *in vitro*. Our studies can guide the rational design of novel therapeutic strategies in treating cardiovascular diseases. It might be possible to maintain chronic myosin activity in pathophysiological conditions without causing debilitating side effects. A deeper understanding of the structural and functional differences between both the cardiac myosin isoforms will enable the application of clinical strategies with increased sophistication. I am hopeful that armed with these biochemical insights, we can improve the lives of cardiovascular diseased patients with novel curative therapeutics.

REFERENCES

[1] T. D. Pollard and E. D. Korn, "Acanthamoeba myosin: I. isolation from acanthamoeba castellanii of an enzyme similar to muscle myosin," *Journal of Biological Chemistry*, vol. 248, no. 13, pp. 4682–4690, 1973.

[2] M. S. Mooseker and R. E. Cheney, "Unconventional myosins," *Annual review of cell and developmental biology*, vol. 11, no. 1, pp. 633–675, 1995.

[3] F. Odronitz and M. Kollmar, "Drawing the tree of eukaryotic life based on the analysis of 2,269 manually annotated myosins from 328 species," *Genome biology*, vol. 8, no. 9, pp. 1–23, 2007.

[4] T. A. McMahon, *Muscles, reflexes, and locomotion*, vol. 10. Princeton University Press, 1984.

[5] C. Batters, C. P. Arthur, A. Lin, J. Porter, M. A. Geeves, R. A. Milligan, J. E. Molloy, and L. M. Coluccio, "Myo1c is designed for the adaptation response in the inner ear," *The EMBO journal*, vol. 23, no. 7, pp. 1433–1440, 2004.

[6] J. A. Hammer and J. R. Sellers, "Walking to work: roles for class v myosins as cargo transporters," *Nature reviews Molecular cell biology*, vol. 13, no. 1, pp. 13–26, 2012.

[7] F. Buss, G. Spudich, and J. Kendrick-Jones, "Myosin vi: cellular functions and motor properties," *Annu. Rev. Cell Dev. Biol.*, vol. 20, pp. 649–676, 2004.

[8] M. Schliwa and G. Woehlke, "Molecular motors," *Nature*, vol. 422, no. 6933, pp. 759–765, 2003.

[9] A. S. Reddy and I. S. Day, "Analysis of the myosins encoded in the recently

completed arabidopsis thaliana genome sequence," *Genome biology*, vol. 2, no. 7, pp. 1–19, 2001.

[10] F. Baluška, F. Cvrčková, J. Kendrick-Jones, and D. Volkmann, "Sink plasmodesmata as gateways for phloem unloading. myosin viii and calreticulin as molecular determinants of sink strength?," *Plant Physiology*, vol. 126, no. 1, pp. 39–46, 2001.

[11] S. Reichelt, A. E. Knight, T. P. Hodge, F. Baluska, J. Samaj, D. Volkmann, and J. Kendrick-Jones, "Characterization of the unconventional myosin viii in plant cells and its localization at the post-cytokinetic cell wall," *The Plant Journal*, vol. 19, no. 5, pp. 555–567, 1999.

[12] V. Ropars, Z. Yang, T. Isabet, F. Blanc, K. Zhou, T. Lin, X. Liu, P. Hissier, F. Samazan, B. Amigues, *et al.*, "The myosin x motor is optimized for movement on actin bundles," *Nature communications*, vol. 7, no. 1, pp. 1–13, 2016.

[13] C. Hettmann, A. Herm, A. Geiter, B. Frank, E. Schwarz, T. Soldati, and D. Soldati, "A dibasic motif in the tail of a class xiv apicomplexan myosin is an essential determinant of plasma membrane localization," *Molecular biology of the cell*, vol. 11, no. 4, pp. 1385–1400, 2000.

[14] R. Lymn and E. W. Taylor, "Mechanism of adenosine triphosphate hydrolysis by actomyosin," *Biochemistry*, vol. 10, no. 25, pp. 4617–4624, 1971.

[15] E. Behrmann, M. Müller, P. A. Penczek, H. G. Mannherz, D. J. Manstein, and S. Raunser, "Structure of the rigor actin-tropomyosin-myosin complex," *Cell*, vol. 150, no. 2, pp. 327–338, 2012.

[16] S. Kühner and S. Fischer, "Structural mechanism of the atp-induced dissociation of rigor myosin from actin," *Proceedings of the National Academy of Sciences*, vol. 108, no. 19, pp. 7793–7798, 2011.

[17] M. Cecchini, Y. Alexeev, and M. Karplus, "Pi release from myosin: a simulation analysis of possible pathways," *Structure*, vol. 18, no. 4, pp. 458–470, 2010.

[18] S. Fischer, B. Windshügel, D. Horak, K. C. Holmes, and J. C. Smith, "Structural mechanism of the recovery stroke in the myosin molecular motor," *Proceedings of the National Academy of Sciences*, vol. 102, no. 19, pp. 6873–6878, 2005.

[19] I. Rayment, H. M. Holden, M. Whittaker, C. B. Yohn, M. Lorenz, K. C. Holmes, and R. A. Milligan, "Structure of the actin-myosin complex and its implications for muscle contraction," *Science*, vol. 261, no. 5117, pp. 58–65, 1993.

[20] K. C. Holmes, I. Angert, F. J. Kull, W. Jahn, and R. R. Schröder, "Electron cryo-microscopy shows how strong binding of myosin to actin releases nucleotide," *Nature*, vol. 425, no. 6956, pp. 423–427, 2003.

[21] J. von der Ecken, S. M. Heissler, S. Pathan-Chhatbar, D. J. Manstein, and S. Raunser, "Cryo-em structure of a human cytoplasmic actomyosin complex at near-atomic resolution," *Nature*, vol. 534, no. 7609, pp. 724–728, 2016.

[22] H. Yu, L. Ma, Y. Yang, and Q. Cui, "Mechanochemical coupling in the myosin motor domain. i. insights from equilibrium active-site simulations," *PLoS Comput Biol*, vol. 3, no. 2, p. e21, 2007.

[23] H. Onishi, S. V. Mikhailenko, and M. F. Morales, "Toward understanding actin activation of myosin atpase: the role of myosin surface loops," *Proceedings of the National Academy of Sciences*, vol. 103, no. 16, pp. 6136–6141, 2006.

[24] M. Furch, B. Remmel, M. A. Geeves, and D. J. Manstein, "Stabilization of the actomyosin complex by negative charges on myosin," *Biochemistry*, vol. 39, no. 38, pp. 11602–11608, 2000.

[25] P. B. Joel, K. M. Trybus, and H. L. Sweeney, "Two conserved lysines at the 50/20-kda junction of myosin are necessary for triggering actin activation," *Journal of Biological Chemistry*, vol. 276, no. 5, pp. 2998–3003, 2001.

[26] Q.-M. Nie, A. Togashi, T. N. Sasaki, M. Takano, M. Sasai, and T. P. Terada, "Coupling of lever arm swing and biased brownian motion in actomyosin," *PLoS Comput Biol*, vol. 10, no. 4, p. e1003552, 2014.

[27] S. S. Margossian and S. Lowey, "Substructure of the myosin molecule: Iii. preparation of single-headed derivatives of myosin," *Journal of molecular biology*, vol. 74, no. 3, pp. 301–311, 1973.

[28] D. Mornet, P. Pantel, E. Audemard, and R. Kassab, "The limited tryptic cleavage of chymotryptic s-1: an approach to the characterization of the actin site in myosin heads," *Biochemical and biophysical research communications*, vol. 89, no. 3, pp. 925–932, 1979.

[29] I. Rayment, W. R. Rypniewski, K. Schmidt-Base, R. Smith, D. R. Tomchick, M. M. Benning, D. A. Winkelmann, G. Wesenberg, and H. M. Holden, "Three-dimensional structure of myosin subfragment-1: a molecular motor," *Science*, vol. 261, no. 5117, pp. 50–58, 1993.

[30] M. J. T. Cope, J. Whisstock, I. Rayment, and J. Kendrick-Jones, "Conservation within the myosin motor domain: implications for structure and function," *Structure*, vol. 4, no. 8, pp. 969–987, 1996.

[31] C. A. Smith and I. Rayment, "Active site comparisons highlight structural similarities between myosin and other p-loop proteins," *Biophysical Journal*, vol. 70, no. 4, pp. 1590–1602, 1996.

[32] A. Houdusse and C. Cohen, "Structure of the regulatory domain of scallop myosin at 2 å resolution: implications for regulation," *Structure*, vol. 4, no. 1, pp. 21–32, 1996.

[33] J. R. Sellers, "Mechanism of the phosphorylation-dependent regulation of smooth muscle heavy meromyosin.," *Journal of Biological Chemistry*, vol. 260, no. 29, pp. 15815–15819, 1985.

[34] M. A. Geeves and K. C. Holmes, "The molecular mechanism of muscle contraction," *Advances in protein chemistry*, vol. 71, pp. 161–193, 2005.

[35] H. L. Sweeney and A. Houdusse, "Structural and functional insights into the myosin motor mechanism," *Annual review of biophysics*, vol. 39, pp. 539–557, 2010.

[36] S. Fujita-Becker, U. Dürrwang, M. Erent, R. J. Clark, M. A. Geeves, and D. J. Manstein, "Changes in mg2+ ion concentration and heavy chain phosphorylation regulate the motor activity of a class i myosin," *Journal of Biological Chemistry*, vol. 280, no. 7, pp. 6064–6071, 2005.

[37] B. H. Várkuti, Z. Yang, B. Kintses, P. Erdélyi, I. Bárdos-Nagy, A. L. Kovács, P. Hári, M. Kellermayer, T. Vellai, and A. Málnási-Csizmadia, "A novel actin binding site of myosin required for effective muscle contraction," *Nature structural & molecular biology*, vol. 19, no. 3, p. 299, 2012.

[38] H. L. Sweeney and E. L. Holzbaur, "Motor proteins," *Cold Spring Harbor perspectives in biology*, vol. 10, no. 5, p. a021931, 2018.

[39] D. V. Trivedi, J. M. Muretta, A. M. Swenson, J. P. Davis, D. D. Thomas, and C. M. Yengo, "Direct measurements of the coordination of lever arm swing and the catalytic cycle in myosin v," *Proceedings of the National Academy of Sciences*, vol. 112, no. 47, pp. 14593–14598, 2015.

[40] J. M. Muretta, K. J. Petersen, and D. D. Thomas, "Direct real-time detection of the actin-activated power stroke within the myosin catalytic domain," *Proceedings of the National Academy of Sciences*, vol. 110, no. 18, pp. 7211–7216, 2013.

[41] J. M. Muretta, J. A. Rohde, D. O. Johnsrud, S. Cornea, and D. D. Thomas, "Direct real-time detection of the structural and biochemical events in the myosin power stroke," *Proceedings of the National Academy of Sciences*, vol. 112, no. 46, pp. 14272–14277, 2015.

[42] H. Gutfreund and D. Trentham, "Energy transformation in biological systems," in *Ciba Found. Symp.*, vol. 31, pp. 69–86, Elsevier/Excerpta Medica Amsterdam, New York, 1975.

[43] J. Sleep and R. Hutton, "Exchange between inorganic phosphate and adenosine 5'-triphosphate in the medium by actomyosin subfragment 1," *Biochemistry*, vol. 19, no. 7, pp. 1276–1283, 1980.

[44] F. A. Kiani and S. Fischer, "Catalytic strategy used by the myosin motor to hydrolyze atp," *Proceedings of the National Academy of Sciences*, vol. 111, no. 29, pp. E2947–E2956, 2014.

[45] B. L. Grigorenko, I. A. Kaliman, and A. V. Nemukhin, "Minimum energy reaction profiles for atp hydrolysis in myosin," *Journal of Molecular Graphics and Modelling*, vol. 31, pp. 1–4, 2011.

[46] F. A. Kiani and S. Fischer, "Advances in quantum simulations of atpase catalysis in the myosin motor," *Current opinion in structural biology*, vol. 31, pp. 115–123, 2015.

[47] C. Veigel, S. Schmitz, F. Wang, and J. R. Sellers, "Load-dependent kinetics of

myosin-v can explain its high processivity," *Nature cell biology*, vol. 7, no. 9, pp. 861–869, 2005.

[48] J. Sleep and R. Hutton, "Actin mediated release of atp from a myosin atp complex," *Biochemistry*, vol. 17, no. 25, pp. 5423–5430, 1978.

[49] E. M. De La Cruz and E. M. Ostap, "Relating biochemistry and function in the myosin superfamily," *Current opinion in cell biology*, vol. 16, no. 1, pp. 61–67, 2004.

[50] M. J. Bloemink and M. A. Geeves, "Shaking the myosin family tree: biochemical kinetics defines four types of myosin motor," in *Seminars in cell & developmental biology*, vol. 22, pp. 961–967, Elsevier, 2011.

[51] N. Kodera, D. Yamamoto, R. Ishikawa, and T. Ando, "Video imaging of walking myosin v by high-speed atomic force microscopy," *Nature*, vol. 468, no. 7320, pp. 72–76, 2010.

[52] E. J. Benjamin, P. Muntner, A. Alonso, M. S. Bittencourt, C. W. Callaway, A. P. Carson, A. M. Chamberlain, A. R. Chang, S. Cheng, S. R. Das, *et al.*, "Heart disease and stroke statisticsâ2019 update: a report from the american heart association," *Circulation*, vol. 139, no. 10, pp. e56–e528, 2019.

[53] B. D. Lowes, W. Minobe, W. T. Abraham, M. N. Rizeq, T. J. Bohlmeyer, R. A. Quaife, R. L. Roden, D. L. Dutcher, A. D. Robertson, N. F. Voelkel, D. B. Badesch, B. M. Groves, E. M. Gilbert, and M. R. Bristow, "Changes in gene expression in the intact human heart. downregulation of alpha-myosin heavy chain in hypertrophied, failing ventricular myocardium," *J Clin Invest*, vol. 100, no. 9, pp. 2315–24, 1997.

[54] H. Lv, E. Havari, S. Pinto, R. V. Gottumukkala, L. Cornivelli, K. Raddassi, T. Matsui, A. Rosenzweig, R. T. Bronson, R. Smith, A. L. Fletcher, S. J. Turley,

K. Wucherpfennig, B. Kyewski, and M. A. Lipes, "Impaired thymic tolerance to α-myosin directs autoimmunity to the heart in mice and humans," *J Clin Invest*, vol. 121, no. 4, pp. 1561–73, 2011.

[55] S. Miyata, W. Minobe, M. R. Bristow, and L. A. Leinwand, "Myosin heavy chain isoform expression in the failing and nonfailing human heart," *Circ Res*, vol. 86, no. 4, pp. 386–90, 2000.

[56] J. James, L. Martin, M. Krenz, C. Quatman, F. Jones, R. Klevitsky, J. Gulick, and J. Robbins, "Forced expression of alpha-myosin heavy chain in the rabbit ventricle results in cardioprotection under cardiomyopathic conditions," *Circulation*, vol. 111, no. 18, pp. 2339–46, 2005.

[57] T. Q. Uyeda, S. J. Kron, and J. A. Spudich, "Myosin step size. estimation from slow sliding movement of actin over low densities of heavy meromyosin," *J Mol Biol*, vol. 214, no. 3, pp. 699–710, 1990.

[58] P. J. Reiser, M. A. Portman, X.-H. Ning, and C. S. Moravec, "Human cardiac myosin heavy chain isoforms in fetal and failing adult atria and ventricles," *American Journal of Physiology-Heart and Circulatory Physiology*, vol. 280, no. 4, pp. H1814–H1820, 2001. PMID: 11247796.

[59] C. M. Yengo, Y. Takagi, and J. R. Sellers, "Temperature dependent measurements reveal similarities between muscle and non-muscle myosin motility," *Journal of Muscle Research and Cell Motility*, vol. 33, pp. 385–394, Dec 2012.

[60] A. M. Swenson, W. Tang, C. A. Blair, C. M. Fetrow, W. C. Unrath, M. J. Previs, K. S. Campbell, and C. M. Yengo, "Omecamtiv mecarbil enhances the duty ratio of human beta-cardiac myosin resulting in increased calcium sensitivity and slowed

force development in cardiac muscle," *J Biol Chem*, vol. 292, no. 9, pp. 3768–3778, 2017.

[61] J. C. Deacon, M. J. Bloemink, H. Rezavandi, M. A. Geeves, and L. A. Leinwand, "Identification of functional differences between recombinant human α and β cardiac myosin motors," *Cellular and Molecular Life Sciences*, vol. 69, no. 13, pp. 2261–2277, 2012.

[62] A. Gargey, J. Ge, Y. V. Tkachev, and Y. E. Nesmelov, "Electrostatic interactions in the force-generating region of the human cardiac myosin modulate adp dissociation from actomyosin," *Biochemical and biophysical research communications*, vol. 509, no. 4, pp. 978–982, 2019.

[63] J. A. Spudich, "How molecular motors work," *Nature*, vol. 372, no. 6506, pp. 515–518, 1994.

[64] S. Kurzawa-Goertz, C. L. Perreault-Micale, K. M. Trybus, A. Szent-Györgyi, and M. A. Geeves, "Loop i can modulate adp affinity, atpase activity, and motility of different scallop myosins. transient kinetic analysis of s1 isoforms," *Biochemistry*, vol. 37, no. 20, pp. 7517–7525, 1998.

[65] C. Perreault-Micale, "Kalabokis vn, nyitray l, and szent-gyorgyi ag," *Sequence variations in the surface loop near the nucleotide binding site modulate the ATP turnover rates of molluscan myosins. J Muscle Res Cell Motil*, vol. 17, pp. 543–553, 1996.

[66] C. T. Murphy and J. A. Spudich, "The sequence of the myosin 50- 20k loop affects myosin's affinity for actin throughout the actin- myosin atpase cycle and its maximum atpase activity," *Biochemistry*, vol. 38, no. 12, pp. 3785–3792, 1999.

[67] M. A. Geeves and K. C. Holmes, "Structural mechanism of muscle contraction," *Annual review of biochemistry*, vol. 68, no. 1, pp. 687–728, 1999.

[68] R. Clark, M. A. Ansari, S. Dash, M. A. Geeves, and L. M. Coluccio, "Loop 1 of transducer region in mammalian class i myosin, myo1b, modulates actin affinity, atpase activity, and nucleotide access," *Journal of Biological Chemistry*, vol. 280, no. 35, pp. 30935–30942, 2005.

[69] N. Adamek, A. Lieto-Trivedi, M. A. Geeves, and L. M. Coluccio, "Modification of loop 1 affects the nucleotide binding properties of myo1c, the adaptation motor in the inner ear," *Biochemistry*, vol. 49, no. 5, pp. 958–971, 2010.

[70] A. Kalganov, N. Shalabi, N. Zitouni, L. H. Kachmar, A.-M. Lauzon, and D. E. Rassier, "Forces measured with micro-fabricated cantilevers during actomyosin interactions produced by filaments containing different myosin isoforms and loop 1 structures," *Biochimica et Biophysica Acta (BBA)-General Subjects*, vol. 1830, no. 3, pp. 2710–2719, 2013.

[71] Y.-S. Cheng, O. S. Matusovskiy, and D. E. Rassier, "Cleavage of loops 1 and 2 in skeletal muscle heavy meromyosin (hmm) leads to a decreased function," *Archives of biochemistry and biophysics*, vol. 661, pp. 168–177, 2019.

[72] H. L. Sweeney, S. S. Rosenfeld, F. Brown, L. Faust, J. Smith, J. Xing, L. A. Stein, and J. R. Sellers, "Kinetic tuning of myosin via a flexible loop adjacent to the nucleotide binding pocket," *Journal of Biological Chemistry*, vol. 273, no. 11, pp. 6262–6270, 1998.

[73] C. T. Murphy and J. A. Spudich, "Variable surface loops and myosin activity: accessories to a motor," *Journal of Muscle Research & Cell Motility*, vol. 21, no. 2, pp. 139–151, 2000.

[74] H. V. Goodson, H. M. Warrick, and J. A. Spudich, "Specialized conservation of surface loops of myosin: evidence that loops are involved in determining functional characteristics," *Journal of molecular biology*, vol. 287, no. 1, pp. 173–185, 1999.

[75] C. R. Bagshaw and D. R. Trentham, "The characterization of myosin-product complexes and of product-release steps during the magnesium ion-dependent adenosine triphosphatase reaction," *Biochem J*, vol. 141, no. 2, pp. 331–49, 1974.

[76] A. Houdusse, V. N. Kalabokis, D. Himmel, A. G. Szent-GyÃ¶rgyi, and C. Cohen, "Atomic structure of scallop myosin subfragment s1 complexed with mgadp: A novel conformation of the myosin head," *Cell*, vol. 97, no. 4, pp. 459 – 470, 1999.

[77] S. Gourinath, D. M. Himmel, J. H. Brown, L. Reshetnikova, A. G. Szent-GyÃ¶rgyi, and C. Cohen, "Crystal structure of scallop myosin s1 in the pre-power stroke state to 2.6 Ã resolution: Flexibility and function in the head," *Structure*, vol. 11, no. 12, pp. 1621 – 1627, 2003.

[78] H. Onishi, T. Ohki, N. Mochizuki, and M. F. Morales, "Early stages of energy transduction by myosin: roles of arg in switch i, of glu in switch ii, and of the salt-bridge between them," *Proceedings of the National Academy of Sciences*, vol. 99, no. 24, pp. 15339–15344, 2002.

[79] M. Furch, S. Fujita-Becker, M. A. Geeves, K. C. Holmes, and D. J. Manstein, "Role of the salt-bridge between switch-1 and switch-2 of dictyostelium myosin," *Journal of molecular biology*, vol. 290, no. 3, pp. 797–809, 1999.

[80] K. Ruppel and J. Spudich, "Structure-function studies of the myosin motor domain: importance of the 50-kda cleft.," *Molecular biology of the cell*, vol. 7, no. 7, pp. 1123–1136, 1996.

[81] S. Wakelin, P. B. Conibear, R. J. Woolley, D. N. Floyd, C. R. Bagshaw, M. Kovács, and A. Málnási-Csizmadia, "Engineering dictyostelium discoideum myosin ii for the introduction of site-specific fluorescence probes," *Journal of Muscle Research & Cell Motility*, vol. 23, no. 7, pp. 673–683, 2002.

[82] H. Onishi, M. F. Morales, S.-i. Kojima, K. Katoh, and K. Fujiwara, "Functional transitions in myosin: role of highly conserved gly and glu residues in the active site," *Biochemistry*, vol. 36, no. 13, pp. 3767–3772, 1997.

[83] N. Sasaki, T. Shimada, and K. Sutoh, "Mutational analysis of the switch ii loop ofdictyostelium myosin ii," *Journal of Biological Chemistry*, vol. 273, no. 32, pp. 20334–20340, 1998.

[84] T. Kambara, T. E. Rhodes, R. Ikebe, M. Yamada, H. D. White, and M. Ikebe, "Functional significance of the conserved residues in the flexible hinge region of the myosin motor domain," *Journal of Biological Chemistry*, vol. 274, no. 23, pp. 16400–16406, 1999.

[85] X.-d. Li, T. E. Rhodes, R. Ikebe, T. Kambara, H. D. White, and M. Ikebe, "Effects of mutations in the γ-phosphate binding site of myosin on its motor function," *Journal of Biological Chemistry*, vol. 273, no. 42, pp. 27404–27411, 1998.

[86] S. Baylor and S. Hollingworth, "Model of sarcomeric ca2+ movements, including atp ca2+ binding and diffusion, during activation of frog skeletal muscle," *The Journal of general physiology*, vol. 112, no. 3, pp. 297–316, 1998.

[87] S. M. Baylor and S. Hollingworth, "Intracellular calcium movements during excitation–contraction coupling in mammalian slow-twitch and fast-twitch muscle fibers," *Journal of General Physiology*, vol. 139, no. 4, pp. 261–272, 2012.

[88] A. Struk, F. Lehmann-Horn, and W. Melzer, "Voltage-dependent calcium release in human malignant hyperthermia muscle fibers," *Biophysical journal*, vol. 75, no. 5, pp. 2402–2410, 1998.

[89] S. Ali, "Taguchi a, rosenberg h," *Malignant hyperthermia. Best Pract Res Clin Anaesthesiol*, vol. 17, pp. 519–533, 2003.

[90] T. R. Cully, J. N. Edwards, and B. S. Launikonis, "Activation and propagation of ca2+ release from inside the sarcoplasmic reticulum network of mammalian skeletal muscle," *The Journal of physiology*, vol. 592, no. 17, pp. 3727–3746, 2014.

[91] K. Luby-Phelps, "The physical chemistry of cytoplasm and its influence on cell function: an update," *Molecular biology of the cell*, vol. 24, no. 17, pp. 2593–2596, 2013.

[92] L. A. Benton, A. E. Smith, G. B. Young, and G. J. Pielak, "Unexpected effects of macromolecular crowding on protein stability," *Biochemistry*, vol. 51, no. 49, pp. 9773–9775, 2012.

[93] H. STRZELECKA-GOLASZEWSKA, E. PRÓCHNIEWICZ, E. NOWAK, S. Zmorzynski, and W. Drabikowski, "Chicken-gizzard actin: polymerization and stability," *European journal of biochemistry*, vol. 104, no. 1, pp. 41–52, 1980.

[94] G. S. Waller, G. Ouyang, J. Swafford, P. Vibert, and S. Lowey, "A minimal motor domain from chicken skeletal muscle myosin," *Journal of Biological Chemistry*, vol. 270, no. 25, pp. 15348–15352, 1995.

[95] T. W. Houk Jr and K. Ue, "The measurement of actin concentration in solution: a comparison of methods," *Analytical biochemistry*, vol. 62, no. 1, pp. 66–74, 1974.

[96] Y. Takagi, Y. Yang, I. Fujiwara, D. Jacobs, R. E. Cheney, J. R. Sellers, and

M. Kovács, "Human myosin vc is a low duty ratio, nonprocessive molecular motor," *Journal of Biological Chemistry*, vol. 283, no. 13, pp. 8527–8537, 2008.

[97] H. Sigel and B. Song, "Solution structures of nucleotide-metal ion complexes. isomeric equilibria," *Metal ions in biological systems*, vol. 32, pp. 135–135, 1996.

[98] N. C. Melchior, "Sodium and potassium complexes of adenosine-triphosphate: equilibrium studies," *Journal of Biological Chemistry*, vol. 208, no. 2, pp. 615–627, 1954.

[99] P. A. Lanzetta, L. J. Alvarez, P. S. Reinach, and O. A. Candia, "An improved assay for nanomole amounts of inorganic phosphate," *Analytical biochemistry*, vol. 100, no. 1, pp. 95–97, 1979.

[100] A. Martonosi, M. Gouvea, and J. Gergely, "Studies on actin: I. the interaction of c14-labeled adenine nucleotides with actin," *Journal of Biological Chemistry*, vol. 235, no. 6, pp. 1700–1703, 1960.

[101] P. Dancker, I. Löw, W. Hasselbach, and T. Wieland, "Interaction of actin with phalloidin:: Polymerization and stabilization of f-actin," *Biochimica et Biophysica Acta (BBA)-Protein Structure*, vol. 400, no. 2, pp. 407–414, 1975.

[102] I. Segel, "Biochemical calculations wiley new york," 1976.

[103] S. S. Rosenfeld, J. Xing, M. Whitaker, H. C. Cheung, F. Brown, A. Wells, R. A. Milligan, and H. L. Sweeney, "Kinetic and spectroscopic evidence for three actomyosin: Adp states in smooth muscle," *Journal of Biological Chemistry*, vol. 275, no. 33, pp. 25418–25426, 2000.

[104] P. Brissette, D. P. Ballou, and V. Massey, "Determination of the dead time of a stopped-flow fluorometer," *Analytical biochemistry*, vol. 181, no. 2, pp. 234–238, 1989.

[105] D. E. Hannemann, W. Cao, A. O. Olivares, J. P. Robblee, and E. M. De La Cruz, "Magnesium, adp, and actin binding linkage of myosin v: Evidence for multiple myosin v- adp and actomyosin v- adp states," *Biochemistry*, vol. 44, no. 24, pp. 8826–8840, 2005.

[106] N. Albet-Torres, M. J. Bloemink, T. Barman, R. Candau, K. Frölander, M. A. Geeves, K. Golker, C. Herrmann, C. Lionne, C. Piperio, *et al.*, "Drug effect unveils inter-head cooperativity and strain-dependent adp release in fast skeletal actomyosin," *Journal of Biological Chemistry*, vol. 284, no. 34, pp. 22926–22937, 2009.

[107] A. Gargey, S. B. Iragavarapu, A. V. Grdzelishvili, and Y. E. Nesmelov, "Electrostatic interactions in the sh1-sh2 helix of human cardiac myosin modulate the time of strong actomyosin binding," *Journal of Muscle Research and Cell Motility*, pp. 1–11, 2020.

[108] R. C. Phillips, S. P. George, and R. Rutman, "Thermodynamic studies of the formation and ionization of the magnesium (ii) complexes of adp and atp over the ph range 5 to 91," *Journal of the American Chemical Society*, vol. 88, no. 12, pp. 2631–2640, 1966.

[109] J. Ge, S. D. Bouriyaphone, T. A. Serebrennikova, A. V. Astashkin, and Y. E. Nesmelov, "Macromolecular crowding modulates actomyosin kinetics," *Biophysical journal*, vol. 111, no. 1, pp. 178–184, 2016.

[110] Y. V. Tkachev, J. Ge, I. V. Negrashov, and Y. E. Nesmelov, "Metal cation controls myosin and actomyosin kinetics," *Protein science*, vol. 22, no. 12, pp. 1766–1774, 2013.

[111] J. Ge, A. Gargey, I. V. Nesmelova, and Y. E. Nesmelov, "Caatp prolongs strong

actomyosin binding and promotes futile myosin stroke," *Journal of muscle research and cell motility*, vol. 40, no. 3, pp. 389–398, 2019.

[112] C. Manno, L. Figueroa, L. Royer, S. Pouvreau, C. S. Lee, P. Volpe, A. Nori, J. Zhou, G. Meissner, S. L. Hamilton, *et al.*, "Altered ca2+ concentration, permeability and buffering in the myofibre ca2+ store of a mouse model of malignant hyperthermia," *The Journal of physiology*, vol. 591, no. 18, pp. 4439–4457, 2013.

[113] T. Q. Uyeda, K. M. Ruppel, and J. A. Spudich, "Enzymatic activities correlate with chimaeric substitutions at the actin-binding face of myosin," *Nature*, vol. 368, no. 6471, pp. 567–569, 1994.

[114] M. Krenz, A. Sanbe, F. Bouyer-Dalloz, J. Gulick, R. Klevitsky, T. E. Hewett, H. E. Osinska, J. N. Lorenz, C. Brosseau, A. Federico, *et al.*, "Analysis of myosin heavy chain functionality in the heart," *Journal of Biological Chemistry*, vol. 278, no. 19, pp. 17466–17474, 2003.

[115] F. I. Malik, J. J. Hartman, K. A. Elias, B. P. Morgan, H. Rodriguez, K. Brejc, R. L. Anderson, S. H. Sueoka, K. H. Lee, J. T. Finer, *et al.*, "Cardiac myosin activation: a potential therapeutic approach for systolic heart failure," *Science*, vol. 331, no. 6023, pp. 1439–1443, 2011.

[116] J. G. Cleland, J. R. Teerlink, R. Senior, E. M. Nifontov, J. J. Mc Murray, C. C. Lang, V. A. Tsyrlin, B. H. Greenberg, J. Mayet, D. P. Francis, *et al.*, "The effects of the cardiac myosin activator, omecamtiv mecarbil, on cardiac function in systolic heart failure: a double-blind, placebo-controlled, crossover, dose-ranging phase 2 trial," *The Lancet*, vol. 378, no. 9792, pp. 676–683, 2011.

APPENDIX A: DIFFERENTIAL EQUATIONS

Differential equations corresponding to the reaction shown in Figure 2.3.

1. $dAM/dt = -k_{+1T}\ AMT + k_{-1T}\ AMT$
2. $dAMT/dt = k_{+1T}\ AMT - k_{-1T}\ AMT - k_{+2T}\ AMT + k_{-2T}\ AMT$
3. $dMT/dt = k_{+2T}\ AMT - k_{-2T}\ AMT$
4. $dA/dt = k_{+2T}AMT - k_{-2T}AMT$

Differential equations corresponding to the reaction shown in Figure 2.4

1. $dAM/dt = -k_{+1T}AMT + k_{-1T}AMT - k_{+1D}AMD + k_{-1D}AMD$
2. $dAMT/dt = k_{+1T}AMT - (k_{-1T} + k_{+2T})AMT + k_{-2T}AMT$
3. $dA/dt = k_{+2T}AMT - k_{-2T}AMT$
4. $dMT/dt = k_{+2T}AMT - k_{-2T}AMT$
5. $dAMD/dt = k_{+1D}AMD - k_{-1D}AMD$
6. $dD/dt = -k_{+1D}AMD + k_{-1D}AMD$

Differential equations were solved numerically using Wolfram Mathematica built-in symbol NDSolve. The solution was fitted to the experimental data using the built-in symbol NMinimize, which searches for a global minimum. Maximum number of iterations was usually set to 100. If minimization was not completed, maximum 200 iterations were used. We first fitted transients from the experiment with [ADP] = 0 (Figure 2.3) to determine reaction rate constants $k_{+1T}, k_{-1T}, k_{+2T}, k_{-2T}$. Transients obtained from the same myosin construct preparation were fitted globally. We used obtained reaction rate constants in the fit of transients, obtained in experiments with [ADP] = 0. All transients obtained in reactions using myosin from the same preparation were fitted globally for all used ADP concentrations. Reaction rate constants determined from the fits for different preparations of the same myosin construct were averaged and reported as mean ± standard deviation.

APPENDIX B: COLLISION COMPLEX FORMATION ANALYSIS OF ACTOMYOSIN-ATP

In the ATP-induced actomyosin dissociation experiment, hyperbolic fit of actomyosin dissociation rates at different ATP concentration produces constant $K_{app} = 1/K_1^{'}$, where $K_1^{'}$ is the equilibrium association constant formation of collision actomyosinÂ·ATP complex. We used determined constants $K_1^{'}$ for actomyosin and MgATP and CaATP and calculated the concentration of collision actomyosin-ATP complex, using following derivation.

$[AM]_0 = [AM] + [AMT]$, where $[AM]_0$ is the initial concentration of actomyosin, [AM] and [AMâT] are concentrations of actomyosin and actomyosin-ATP complex in mixture, $[T]_0 = [T] + [AMT]$, where $[T]_0$ is the initial concentration of ATP, [T] and $[AMT]$ are concentrations of ATP and actomyosin-ATP complex in mixture, $K_{app} = ([AM][T])/[AMT]$, where K_{app} is the dissociation constant of the collision actomyosin-ATP complex, $1/K_1^{'}$. Then, $K_{app} = (([AM]_0 - [AMT])([T]_0 - [AMT]))/[AMT]$, this equation is rearranged into the quadratic equation $[AMT]^2 - [AMT]([AM]_0 + [T]_0 + K_{app}) + [AM]_0[T]_0 = 0$, with a meaningful solution

$$[AMT] = ((([AM]_0 + [T]_0 + K_{app}) \sqrt{([AM]_0 + [T]_0 + K_{app})^2 - 4[AM]_0[T]_0}))/2.$$